A Decentralized Composite Controller for Unified Voltage Control With Global System Large-Signal Stability in DC Microgrids

Pengfeng Lin, *Student Member, IEEE*, Chuanlin Zhang, *Member, IEEE*, Peng Wang, *Fellow, IEEE*, and Jianfang Xiao, *Member, IEEE*

***Abstract*—Bus voltage control is an essential issue in a DC microgrid (MG). In this paper, a decentralized composite controller (DCC) is proposed to unify two types of voltage controls, i.e., constant voltage mode and droop mode, and simultaneously realize global system large-signal stability of the MG. The main idea of the DCC is to partition the MG into dispatchable unit (DU) subsystems and the lumped load. A well-devised high gain observer is adopted to estimate the electrical coupling of a particular DU subsystem with other DUs and the load. Then, rather than dealing with the MG as a whole, the DCC is locally designed to offset the estimated coupling and stabilize the internal states of the DU subsystem. By doing so, each subsystem can be virtually decoupled from the MG and functions in an isolated fashion. When DU subsystems are interlinked, large-signal stabilization of the entire MG would be obtained by only guaranteeing the localized stability of individual subsystems. This stabilizing strategy has not been reported in the literature thus far. Relevant theoretical analyses are rigorously conducted by employing Lyapunov stability theorem. The effectiveness of the DCC has been verified by simulations. Experimentations show that the DCC enables faster system performance recovery and provides wider stability margin than the conventional PI controller.**

***Index Terms*—Unified voltage control, decentralized controller, large-signal stability, DC microgrids.**

I. Introduction

ENCOURAGED by rapid technological advancements in power electronics, diverse renewable energy sources (RESs) are integrated into existing electrical power systems. Microgrids (MGs), which have variant architectures, offer a flexible way to interconnect these RESs and maximize their advantages. In general, MGs can be categorized into AC MGs and DC MGs. It has been widely admitted that AC power delivery plays a dominant role in traditional generation, transmission, and distribution networks. Despite this fact, extensive attentions have been paid to DC MGs because of the proliferation of DC power consumers, such as LED lights, computers and communication apparatus, etc. These DC consumers are estimated to account for over 80% of the household loads in 10-15 years [1]. Besides, DC compatible energy storages (ESs) also promote the DC MG developments.

In a given DC MG, the bus voltage is a natural indicator of power quality and overall system stability. Hence, appropriate DC bus control is an essential issue and could be realized by those dispatchable units (DUs) such as ESs and DC generators, etc. [2]. Normally, the bus control includes constant voltage mode (CVM) and droop mode (DM). The former can be configured to supply power to voltage-sensitive loads with high power quality requirements. A DU source regulated by CVM should bear sufficient power rating to accommodate all the possible loading conditions [3]. However, in the case that the demanded load power substantially grows, to avoid the overstress of a particular DU, DM should be utilized and implemented for multiple DUs. Then the load can be proportionally shared by different DUs in accordance with their respective ratings. By means of DM, the DC bus voltage will float along with load variations, which means that the heavier loads give the larger voltage drops, and vice versa [4].

For DC DUs, the realizations of CVM and DM significantly rely on their properly controlled interfacing converters. These converters help to feed resistive loads and constant power loads (CPLs). The former ones are known as passive components which contribute damping effects to the MG. Dissimilarly, CPLs are commonly referred to those power electronic loads and motors with tightly regulated speed, etc. They present negative impedances to the DC bus within their control bandwidths, and unfavorably interact with source converters, thus threatening the stable operations of the MG [5]. Furthermore, droop controllers virtually increase the converter output impedances, which further escalates the source-load interactions and entails the bus voltage being more vulnerable

Manuscript received April 1, 2018; revised August 31, 2018; accepted October 6, 2018. Date of publication October 10, 2018; date of current version August 21, 2019. This work was supported in part by the Project Renewable Energy Integration Demonstrator–Singapore in Energy Research Institute @ Nanyang Technological University, in part by the National Natural Science Foundation of China under Grant 61503236, and in part by the Chenguang Program by Shanghai Education Development Foundation and Shanghai Municipal Education Commission under Grant 15CG56. Paper no. TSG-00503-2018. *(Corresponding author: Chuanlin Zhang.)*

P. Lin and J. Xiao are with the Energy Research Institute, Nanyang Technological University, Singapore 637141 (e-mail: linp0010@e.ntu.edu.sg; jfxiao@ntu.edu.sg).

C. Zhang is with the College of Automation Engineering, Shanghai University of Electric Power, Shanghai 200090, China (e-mail: clzhang@shiep.edu.cn).

P. Wang is with the School of Electrical and Electronic Engineering, Nanyang Technological University, Singapore 639798 (e-mail: epwang@ntu.edu.sg).

Color versions of one or more of the figures in this paper are available online at http://ieeexplore.ieee.org.

Digital Object Identifier 10.1109/TSG.2018.2875165

TABLE I
COMPARISONS BETWEEN DCC AND EXISTING STABILIZATION METHODS

References	Model linearization at certain equilibriums (SSA)	No localized linearization (LSA)	Only individual DU converter model needed	The complete model of entire MG needed	Neglecting some of nonlinearities	Self-disciplined stabilization
[7], [8]	√	×	×	√	×	×
[5], [9], [10]			√	×	×	√
[11], [12]			×	√	×	×
[13], [14]			√	×	×	√
[15], [16]	×	√	√	×	×	×
[17]			√	×	√	×
[18], [19]			×	√	√	×
[20]			×	√	×	×
Proposed DCC			√	×	×	√

to load variations [6]. To address these problems, abundant stabilization studies have been conducted using either small-signal analyses (SSA) or large-signal analyses (LSA).

The philosophy of SSA is to establish the linearized mathematical model of the MG, such as the state space model and the transfer function, at an equilibrium under a small perturbation. For examples, in [7] and [8], the eigenvalue loci of a linearized aircraft power system model are analyzed to predict the maximum allowable loads. Note that the eigenvalue method can only be executed off-line, and the entire MG system accurate model is necessitated. A low pass filter based droop controller is proposed in [9] to form virtual impedances for source converters, intending to widen the stability margin of the MG in the small-signal sense. Similarly, a virtual inductor is presented in [10] to damp the potential DC power oscillations by modifying the system transfer function, whereas in [5], a virtual resistor is adopted. Since these virtual impedance method enabled controls are only evaluated in each individual DU converter, the controls certainly take the advantages of high scalability and PnP functionalities. A cubature Kalman filter (CKF) approach is proposed in [11] to improve the small-signal stabilization of nonlinear DC loads. Yet this approach can only be implemented in a central controller which needs intensive communications across the whole MG, and the convergence of CKF necessitates MG models with high accuracy. A small-signal model of a DC MG feeding CPLs is obtained in [12]. The model is utilized to examine the equilibrium existence of the DC system and predict the MG qualitative behavior around a given equilibrium. However, the method in [12] requires complete information of a system with known configurations, and it may not adapt to those MGs with high variable structures. To stabilize the DC MG under changing structures, a better choice is to decompose the MG stabilization target into the DU level; as long as each DU is stabilized properly, the entire DC MG could be stable. This concept is termed as "self-disciplined stabilization" by [13], wherein a passivity based control (PBC) is studied with SSA to reshape converter output impedance, thus increasing the MG damping in the small-signal sense. Similar efforts can also be found in [14] where the impacts of DU output current, input voltage and voltage reference on system passivity are all considered. Conceding that SSA is simple and viable, nevertheless, the locally linearized model is only true in the small vicinity of a steady point. However, the DC MG may have changing equilibriums as it incorporates numerous RESs featured by intermittencies and DUs with plug and play (PnP) properties. The above stabilization controllers would not be valid in full operation ranges.

On the contrary, LSA attempts to study the nonlinear system adopting Lyapunov techniques without localized linearization. With this benefit, a MG equipped with the stabilizer designed by LSA can resist large external disturbances such as unexpected faults, hardware protection and load connection/ disconnection, etc. [21]. A Kalman filter (KF) based network impedance estimation method is proposed in [15] to identify the large-signal operating region in real time. But this process may increase online computational burdens, and the KF algorithm is also sensitive to system parameters. A LSA stabilizer enabled by a virtual capacitor is reported in [16] to stabilize a DC link. The stabilizer is actually based on fuzzy modeling approaches. It is worth noting that the controllers mentioned in [15] and [16] only consider a single converter model, and they may not be suitable for MG applications since analysis intricacies exponentially increase when the MG constantly scales up. To suppress the underlying resonance of a LCL-type voltage source converter (VSC), an auxiliary large-signal stabilizer is employed to ameliorate the VSC control diagram [17]. Nevertheless, only parts of the model states are involved in solving Lyapunov function, and hence, the stabilization of the entire system is not realized. In [18], a virtual impedance control is proposed, and the control method makes a trade-off between the CPL dynamic performances and the output voltage controls of DU systems. Although it helps to alleviate the destabilizing effects of CPL, the nonlinearities of source converters are neglected, which is not feasible in practice. In [19], fuzzy logic is employed to revise current control loop for inverter-dominated AC MG. Despite that fuzzy control law enables inverters to tolerate large disturbance, however, similar to [18], the controller only considers the linear parts of MG system and converter nonlinearities are unluckily neglected. Moreover, the necessary proof of the system large-signal stability is not provided. In [20], a robust voltage control scheme is stated to function in a decentralized way, and the scheme can decently control the bus voltage by rejecting large disturbances. Yet the controller designs substantially hinge on global data collection of the complete MG model through communications. This weakness unfavorably compromises the system scalability, and the centralized

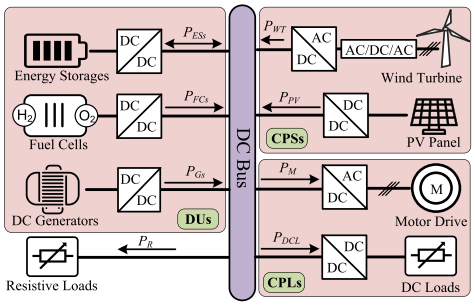

Fig. 1. A generic layout of an autonomous DC microgrid.

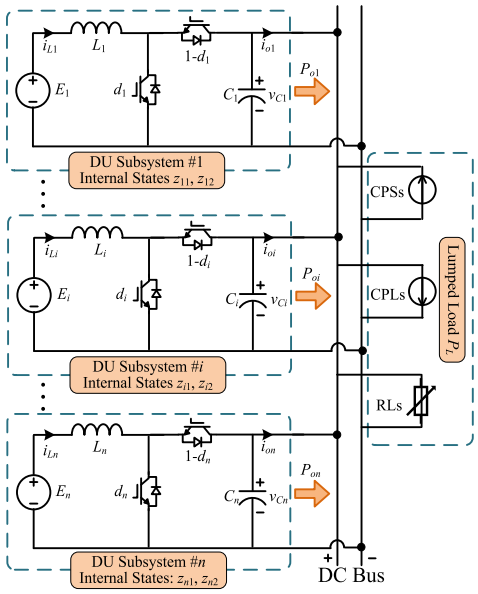

Fig. 2. Detailed DU configurations feeding the lumped load.

controller design process is possibly undermined by single point communication failures. Some other LSA tools such as Brayton-Moser's Mixed Potential and Reverse Trajectory Tracking, can also be found in [21] and [22] etc. These tools merely give the attraction domain of a dynamic system in a specified steady state. In addition, a common characteristic of the above LSA methods is that they would be confined to simple model analyses. The complete model of a large-scale system has to be greatly reduced if the LSA is a necessity. For the DC MG with a growing number of sources/loads, these approaches cannot keep pace with the MG evolutions and may suffer from severe difficulties.

To avoid unnecessary compromises to model completeness and make LSA more applicable to the DC MG with amounting complexities, a decentralized composite controller (DCC) is proposed in this paper to unify both CVM and DM. Each DU, as well as its interfacing converter, constitute a subsystem. For easy explanations, similar to [23] and [24], RESs are emulated as constant power sources (CPSs). These CPSs together with resistive loads and CPLs are merged into the equivalent lumped load which would be fed by DUs. In this context, the electrical coupling of a particular DU subsystem with other subsystems/ loads is firstly estimated by a well-devised high gain observer [25]. Then, instead of directly dealing with the DC MG as a whole, the DCC is individually designed to counteract the observed coupling and simultaneously stabilize the internal states of each subsystem in the large-signal sense. By doing so, each DU subsystem is decoupled from one another and operates in an isolated way from the perspectives of control and stability. When those subsystems are interconnected, the global system large-signal stability of the entire MG can be achieved by simply ensuring the local stabilities of individual subsystems. Hence, the DCC based stabilization scheme is fully decentralized, which remarkably enhances the flexibility and scalability of the MG. Besides, the proposed DCC makes a breakthrough that the tradeoff between dynamic model integrity and LSA could be subtly circumvented. Comprehensive comparisons between the DCC and those existing methods have been summarized in TABLE I, which helps to better illustrate the contribution of this paper.

Following the introduction, electrical coupling concepts are elaborated in Section II. Section III presents the proposed DCC for unified controls of the DC bus voltage (CVM and DM). Then global system large-signal stability of the entire MG is theoretically analyzed through Lyapunov techniques. Section IV provides some discussions on the DCC performances and the DC MG architecture. The DCC effectiveness is verified in Section V by MATLAB simulations. Section VI experimentally compares the performances of the DCC and the traditional PI (Proportional-Integral) controller. The results show that the proposed control law can withstand large system disturbances and expand the MG stability margin. Finally, conclusions are drawn in Section VII.

II. System Description and Coupling Elaboration

A. DC MG Configuration

Fig. 1 plots a generic schematic of an autonomous DC MG wherein all electrical devices are classified into four groups, resistive loads (RLs), CPSs, CPLs and DUs. RLs can be directly linked to the DC bus without any interlinking converters. CPSs are referred to RESs, such as solar PV and wind turbines, which are operated under maximum power point tracking (MPPT) modes to harvest clean energy. Power electronic loads and motor drives can be viewed as CPLs which absorb power from the DC bus regardless of voltage deviations. It should be noted that CPSs and CPLs stem from power control schemes; their correct operations highly necessitate a stable and reliable DC bus. For this purpose, DUs should be configured to realize the designated bus controls, i.e., CVM and DM, respectively.

Proceeding to Fig. 2, to facilitate the system modeling, CPSs, CPLs and resistors can be amalgamated and expressed as the lumped load P_L,

$$P_L(t) = P_{CPLs}(t) + P_{RLs}(t) - P_{CPSs}(t) \tag{1}$$

where $P_{CPLs}(t)$, $P_{RLs}(t)$, and $P_{CPSs}(t)$ are the variables with respect to time t.

From the small-signal point of view, the linearized form of a CPS consists of a positive resistor and a current source.

Therefore, as reported in [23], CPSs help to widen the MG stability margin and may also counterbalance the destabilization effects incurred by CPLs. In a practical MG, the power requested by the lumped load should be completely compensated by a single DU or several DUs. This means that, in the case of CPS generations exceeding the total consumption of CPLs and RLs, P_L in (1) would be a negative value. The surplus power induced in the system, in principle, should be stored by the ES-based DUs so that unnecessary power losses could be avoided. However, this favorable scenario will be purposely excluded from this paper as CPSs would not undermine the system stability. Instead, the subsequent context mainly concentrates on designing the large-signal stabilizer for the MG, and hence, worse situations, like P_L being dominated by CPLs, will be considered.

B. Coupling Elaboration

As emphasized earlier, a DU which has enough capacity for picking up all the loads should be controlled by CVM to minimize bus voltage deviations and improve the overall power quality. For this situation, no additional DU is needed. Taking the first DU in Fig. 2 as an example, the DU helps to construct a slack DC bus for the MG. This means that the power delivered by the DU subsystem completely depends on P_L variations. The increased/decreased P_L will draw more/less power from the source, which consequently causes the inductor current i_{L1} to rise/fall. In this sense, it is reasonable to conceive that the output power P_{o1} represents the electrical coupling between the DU subsystem and the lumped load.

On the other hand, when a single DU with limited capacity cannot supply the load, multiple DUs should be scheduled and work in DMs (see Fig. 2). By using droops, all DUs are allowed to participate in bus voltage controls according to their respective power ratings. Similar to the scenario in CVM, for the ith DU subsystem, its electrical coupling with other subsystems and loads, should be quantified as its contributed power based on proportional power sharing rules.

Regarding a particular subsystem with either CVM or DM, if the coupling mentioned above could be precisely estimated and then neutralized in a certain way, the DU subsystem can be virtually segregated from the MG. Thanks to this scheme, system level stabilization task can be decomposed into the stabilization of each subsystem. Concretely, as long as the internal states residing in DU subsystems are individually stabilized in the large-signal sense, the global system stability of the whole MG can thus be guaranteed. These original concepts highly feature the proposed DCC, and it will be meticulously explicated from the next section onward.

III. Decentralized Composite Controller Design

A. Canonical DU Modeling

As detailed in Fig. 2, the averaged model of the ith boost converter can be expressed as,

$$\dot{i}_{Li} = \frac{E_i}{L_i} - \frac{1-d_i}{L_i} v_{Ci}, \dot{v}_{Ci} = \frac{1-d_i}{C_i} i_{Li} - \frac{P_{oi}}{C_i v_{Ci}}, \tag{2}$$

where i_{Li} and v_{Ci} are the instantaneous inductor current and capacitor voltage. d_i is the duty cycle generated by the controller. E_i denotes the input voltage. Variables accompanied by the subscript "i" mean that they are associating with the ith DU subsystem. The average model describes the converter dynamics in the switching period while the high frequency impacts are neglected [26]. The model hence is tenable regardless of different switching frequencies, and this assumption is widely accepted by a plethora of studies.

Observing from (2), it is easy to find bilinear terms that couple the control input d_i and the states i_{Li}, v_{Ci}. To cope with this tricky nonlinearity, as indicated by [27], the exact feedback linearization should be performed. With a coordinate transformation, equation (2) could be represented by the two new states which are the total energy stored by the converter and the converter input power, respectively. The first state z_{i1} can be constructed as below,

$$z_{i1} = 0.5 L_i i_{Li}^2 + 0.5 C_i v_{Ci}^2. \tag{3}$$

Computing the derivative of z_{i1} yields,

$$\dot{z}_{i1} = L_i i_{Li} \dot{i}_{Li} + C_i v_{Ci} \dot{v}_{Ci} = E_i i_{Li} - P_{oi}. \tag{4}$$

Taking $E_i i_{Li}$ as the second state z_{i2}, its dynamic is given as,

$$\dot{z}_{i2} = u_i = E_i \dot{i}_{Li} = \frac{E_i^2}{L_i} - \frac{1-d_i}{L_i} E_i v_{Ci}. \tag{5}$$

Combining (4) and (5), new dynamics can be obtained,

$$\dot{z}_{i1} = z_{i2} + \varsigma_i, \dot{z}_{i2} = u_i, \tag{6}$$

where $\varsigma_i = -P_{oi}$ denotes the aforementioned coupling imposed by outside electrical components to the ith DU subsystem. u_i is the equivalent control signal, from which the duty cycle d_i in (2) can be accordingly derived as,

$$d_i = 1 - \frac{E_i}{v_{Ci}} + \frac{L_i u_i}{E_i v_{Ci}}. \tag{7}$$

To realize unified voltage control, the objective of d_i is to drive v_{Ci} stably tracking the voltage reference. However, the scenario would be different with the new state variables. For (6), the intention is to design a control input u_i such that z_{i1} enables to practically approach its reference z_{i1r} which is

$$z_{i1r} = 0.5 L_i i_{Lir}^2 + 0.5 C_i v_{Cir}^2 = 0.5 L_i \left(\frac{-\varsigma_i}{E_i} \right)^2 + 0.5 C_i v_{Cir}^2. \tag{8}$$

In (8), v_{Cir} represents the output voltage reference. It could be a constant in CVM, or determined by a droop controller in DM. For the latter, v_{Cir} can be written below,

$$v_{Cir} = V^* - m_i P_{oi} = V^* + m_i \varsigma_i \tag{9}$$

where V^* is the nominal DC bus voltage, and m_i is the droop coefficient of the ith DU subsystem. It is essential to emphasize that the input voltage E_i is a measured value given by a voltage transducer. Assuming that the transducer can reflect E_i dynamic with high fidelity, the real-time variation of E_i could be fully materialized in the canonical modeling. Thus, E_i dynamic would not vitiate the subsequent conclusions concerning the MG stabilization made by DCC.

B. High Gain Observer Design

Comparing (2) and (6) shows that the inborn nonlinear model of the boost converter has been converted into a linear one, which substantially facilitates the large-signal stabilizer design. Unfortunately, dynamics described by (6) are affected by ς_i that is exactly the additive inverse of the output power. The presence of ς_i may severely threaten the tracking performances and even impair the system stability. In addition, it is visible from (8) that the calculation of reference z_{i1r} also involves the coupling. On these bases, it is imperative to know the precise value of ς_i and further process it appropriately in the control law. To this end, a high gain observer is devised as the following [25],

$$\begin{cases} \dot{\hat{z}}_{i11} = z_{i2} + \hat{z}_{i12} + l_{i1}\sigma_i\left(z_{i1} - \hat{z}_{i11}\right) \\ \dot{\hat{z}}_{i12} = \hat{z}_{i13} + l_{i2}\sigma_i^2\left(z_{i1} - \hat{z}_{i11}\right) \\ \dot{\hat{z}}_{i13} = l_{i3}\sigma_i^3\left(z_{i1} - \hat{z}_{i11}\right) \end{cases}, \tag{10}$$

where $\hat{z}_{i11}, \hat{z}_{i12}, \hat{z}_{i13}$ are the estimates of $z_{i1}, \varsigma_i, \dot{\varsigma}_i$. $\sigma_i > 1$ is a positive scaling gain which will be identified later. $H_i = \mathrm{Col}(l_{i1}, l_{i2}, l_{i3})$ is an observer gain vector with its components being corresponding to the coefficients of a Hurwitz polynomial,

$$p_i(s) = s^3 + l_{i1}s^2 + l_{i2}s + l_{i3}. \tag{11}$$

From a practical point of view, P_{oi} has its physical meaning, and it would not go to infinity in the real engineering. Therefore, the derivatives of ς_i should be limited in bounded ranges, which can be mathematically delineated below,

$$\max_{i\le n, j=1,2}\left\{\sup\left|\frac{\partial \varsigma_i^{\,j}}{\partial t^j}\right|\right\} \le D, D \in R_+. \tag{12}$$

Combining (6) and (10) with the denotations $e_{i1} = z_{i1} - \hat{z}_{i11}$ $e_{i2} = (\varsigma_i - \hat{z}_{i12})/\sigma_i$, $e_{i3} = (\dot{\varsigma}_i - \hat{z}_{i13})/\sigma_i^2$, error dynamics can be acquired as,

$$\dot{\boldsymbol{e}}_i = \sigma_i \boldsymbol{A}_i \boldsymbol{e}_i + \boldsymbol{B}_i \ddot{\varsigma}_i, \tag{13}$$

where $\boldsymbol{e}_i = [e_{i1}\ e_{i2}\ e_{i3}]^T$ is the error vector. $\boldsymbol{A}_i = [-l_{i1}\ 1\ 0; -l_{i2}\ 0\ 1; -l_{i3}\ 0\ 0;]$ and $\boldsymbol{B}_i = [0\ 0\ \sigma_i^{-2}]^T$ represent the system matrices. Referring to (11), $\boldsymbol{A}_i$ is a Hurwitz matrix [28]. Hence, there must exist a symmetrical and positive definite matrix $\boldsymbol{Q}_i$ satisfying $\boldsymbol{Q}_i^T\boldsymbol{A}_i + \boldsymbol{A}_i\boldsymbol{Q}_i + \boldsymbol{I} = 0$. Next, it will be shown that error dynamics can be stabilized at the origin if σ_i is properly tuned, which suggests that, $\hat{z}_{i11}, \hat{z}_{i12}, \hat{z}_{i13}$ enable to practically track $z_{i1}, \varsigma_i, \dot{\varsigma}_i$. To this end, constructing a Lyapunov function $V_{ei} = \boldsymbol{e}_i^T\boldsymbol{Q}_i\boldsymbol{e}_i$ whose time derivative along its trajectory is given by,

$$\begin{aligned} \dot{V}_{ei} &= \sigma_i \frac{\partial V_{ei}}{\partial \boldsymbol{e}_i^T}\boldsymbol{A}_i\boldsymbol{e}_i + \frac{\partial V_{e_1}}{\partial \boldsymbol{e}_i^T}\boldsymbol{B}_i\ddot{\varsigma}_i = -\sigma_i\|\boldsymbol{e}_i\|^2 + 2\boldsymbol{e}_i^T\boldsymbol{Q}_i\boldsymbol{B}_i\ddot{\varsigma}_i \\ &\le -\sigma_i\|\boldsymbol{e}_i\|^2 + 2\gamma_i\|\boldsymbol{e}_i\|, \end{aligned} \tag{14}$$

where $\gamma_i = \sigma_i^{-2}\lambda_{\max}(\boldsymbol{Q}_i)D$ and $\lambda_{\max}(\boldsymbol{Q}_i)$ denotes the maximum eigenvalue of $\boldsymbol{Q}_i$.

With the completion of squares, the following inequality holds,

$$2\gamma_i\|\boldsymbol{e}_i\| \le \|\boldsymbol{e}_i\|^2 + \gamma_i^2. \tag{15}$$

Substituting (15) into (14) yields,

$$\begin{aligned} \dot{V}_{ei} &\le -(\sigma_i - 1)\|\boldsymbol{e}_i\|^2 + \gamma_i^2 \\ &\le -(\sigma_i - 1)\lambda_{\max}^{-1}(\boldsymbol{Q}_i)V_{ei} + \gamma_i^2. \end{aligned} \tag{16}$$

Defining $\Omega_{\varepsilon i} = \{\boldsymbol{e}_i \in R^3 | V_{ei} \le \varepsilon_i\}$ where $\varepsilon_i > 0$ is a constant which can be arbitrarily small, it is apparent that $\Omega_{\varepsilon i} \subset R^3$. Noting that σ_i is independent of γ_i, a sufficiently large σ_i can be selected to satisfy

$$\gamma_i^2 \le 0.5(\sigma_i - 1)\lambda_{\max}^{-1}(\boldsymbol{Q}_i)\varepsilon_i. \tag{17}$$

Then, for any $\boldsymbol{e}_i \in (R^3 \backslash \Omega_{\varepsilon i})$ and thereby $V_{ei} \ge \varepsilon_i$, (16) can be rearranged as,

$$\dot{V}_{ei} \le -(\sigma_i - 1)\lambda_{\max}^{-1}(\boldsymbol{Q}_i)\varepsilon_i + \gamma_i^2. \tag{18}$$

With the substitution of (17) into (18), slightly manipulating (18) gives the following,

$$\dot{V}_{ei} \le -0.5(\sigma_i - 1)\lambda_{\max}^{-1}(\boldsymbol{Q}_i)\varepsilon_i < 0. \tag{19}$$

As implied by (19), the derivative of Lyapunov function for the errors can be rigorously negative in the case of $V_{ei} \ge \varepsilon_i$. Moreover, by scrutinizing (17), σ_i and ε_i are inversely correlated. When γ_i keeps unchanged, the increased σ_i leads to the decreased ε_i. Hence, it is possible to adequately magnify σ_i so that ε_i almost equals zero, which means $\Omega_{\varepsilon i}$ can be infinitesimal and consequently $\boldsymbol{e}_i$ can be regulated as small as possible. In this sense, based on (10), it is rational to replace ς_i in (8) and (9) with the estimated value $\hat{z}_{i12}$, which can be expressed as,

$$z_{i1r} = 0.5L_i\left(\frac{-\hat{z}_{i12}}{E_i}\right)^2 + 0.5C_i v_{Cir}^2, \tag{20}$$

$$v_{Cir} = V^* + m_i\hat{z}_{i12}. \tag{21}$$

C. Decentralized Composite Controller Design

Section III-B has presented a well-devised observer to estimate the electrical coupling between the ith DU system and the externals. The estimated quantity can now be employed to accomplish the proposed composite controller design. For that, intermediate states should be introduced first. These states are defined as,

$$\xi_{i1} = z_{i1} - z_{i1r}, \xi_{i2} = (z_{i2} - z_{i2r})/\beta_i, v_i = (u_i - u_{ir})/\beta_i^2, \tag{22}$$

where $\beta_i > 1$ is a positive scaling factor which will be made precisely later. v_i is an auxiliary control input. z_{i1r} has been given by (20). z_{i2r} and u_{ir} are the reference signals for z_{i2} and u_i, which are given below,

$$z_{i2r} = \dot{z}_{i1r} - \hat{z}_{i12}, u_{ir} = \ddot{z}_{i1r} - \hat{z}_{i13}. \tag{23}$$

Regarding the first two equations in (22), it is evident that z_{i1} and z_{i2} are equal to their references z_{i1r} and z_{i2r} in the case that the intermediate states reduce to zero. Accordingly, the boost converter output voltage v_{Ci} can also be forced to track v_{cir}, which is the ultimate objective of this paper. For better understanding this scheme, the derivatives of ξ_{i1} and ξ_{i2} can be computed as,

$$\dot{\xi}_{i1} = \beta_i\xi_{i2} + \sigma_i e_{i2}, \dot{\xi}_{i2} = \beta_i v_i + l_{i2}\sigma_i^2 e_{i1}/\beta_i. \tag{24}$$

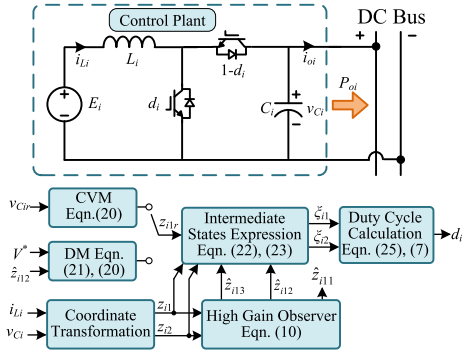

Fig. 3. Control diagram of the proposed DCC for unified voltage control.

To stabilize the above dynamics, v_i could be designed as the linear combination of ξ_{i1} and ξ_{i2}, i.e., $-k_{i1}\xi_{i1} - k_{i2}\xi_{i2}$. k_{i1} and k_{i2} are positive constants. Then the equivalent control u_i as in (6) can be expressed as,

$$u_i = -\beta_i^2(k_{i1}\xi_{i1} + k_{i2}\xi_{i2}) + u_{ir}, \tag{25}$$

For (24), the compact form of the close loop system can be described as,

$$\dot{\boldsymbol{\xi}}_i = \beta_i \boldsymbol{\Lambda}_i \boldsymbol{\xi}_i + \boldsymbol{\Phi}_i, \tag{26}$$

where $\boldsymbol{\xi}_i = [\xi_{i1}\ \xi_{i2}]^T$. $\boldsymbol{\Lambda}_i = [0\ 1; -k_{i1}\ -k_{i2};]$ and $\boldsymbol{\Phi}_i = [\sigma_i e_{i2}\ l_{i2}\sigma_i^2 e_{i1}/\beta_i]^T$ are the system matrices. It should be mentioned that all the derivations of z_{i1r}, z_{i2r} and u_{ir} involve the estimated values $\hat{z}_{i11}$, $\hat{z}_{i12}$ and $\hat{z}_{i13}$. These values will eventually appear in the duty cycle expression with the substitution of u_i in (25) into (7), which gives rise to the formation of "composite controller". With this controller, the impacts of coupling ς_i on tracking performances of the system (6) can be nearly eliminated. Moreover, the proposed controller is completely decentralized which only contains the local state information of the ith DU subsystem. Hence, the flexibility, reliability and PnP functionality of the whole system can be considerably fortified. The detailed control diagram of the DCC are illustrated in Fig. 3.

D. Global System Stability in the Large-Signal Sense

As outlined in the introduction, the DCC allows large-signal stabilization for the entire DC MG. The main feature of the proposed controller is that the global system stability in the large-signal sense can be ensured if all subsystems are individually stabilized. To justify these discussions, relevant theoretical analyses will be provided in this subsection, which could be divided into two steps.

Step1: In the entire DC MG system, any trajectory of all the intermediate states will be uniformly bounded.

For the ith close loop subsystem (26), choosing a Lyapunov function $W_i = \boldsymbol{\xi}_i^T \boldsymbol{P}_i \boldsymbol{\xi}_i$ where $\boldsymbol{P}_i$ is a positive definite and symmetrical matrix subjected to $\boldsymbol{P}_i^T\boldsymbol{\Lambda}_i + \boldsymbol{\Lambda}_i\boldsymbol{P}_i + \boldsymbol{I} = 0$, the derivative of W_i is computed as,

$$\begin{aligned}\dot{W}_i &= \beta_i \frac{\partial W_i}{\partial \boldsymbol{\xi}_i^T}\boldsymbol{\Lambda}_i\boldsymbol{\xi}_i + \frac{\partial W_i}{\partial \boldsymbol{\xi}_i^T}\boldsymbol{\Phi}_i = -\beta_i\|\boldsymbol{\xi}_i\|^2 + 2\boldsymbol{\xi}_i^T\boldsymbol{P}_i\boldsymbol{\Phi}_i \\ &\le -\beta_i\|\boldsymbol{\xi}_i\|^2 + 2\sqrt{\Delta_i}\|\boldsymbol{\xi}_i\|,\end{aligned} \tag{27}$$

where $\sqrt{\Delta_i} = \lambda_{\max}(\boldsymbol{P}_i) \parallel \boldsymbol{\Phi}_i \parallel$ and $\lambda_{\max}(\boldsymbol{P}_i)$ is the maximum eigenvalue of $\boldsymbol{P}_i$. Similar to (15), manipulating (27) yields,

$$\dot{W}_i \le -(\beta_i - 1)\|\boldsymbol{\xi}_i\|^2 + \Delta_i \tag{28}$$

With regard to the MG in Fig. 2, a Lyapunov function for the whole system can be written as

$$W = \boldsymbol{\xi}_\Gamma^T \boldsymbol{P} \boldsymbol{\xi}_\Gamma = \sum_{i=1}^{n} W_i \tag{29}$$

where $\boldsymbol{\xi}_\Gamma = [\boldsymbol{\xi}_1^T \cdots \boldsymbol{\xi}_i^T \cdots \boldsymbol{\xi}_n^T]^T$ and $\boldsymbol{P} = \mathrm{diag}\{\boldsymbol{P}_1 \cdots \boldsymbol{P}_i \cdots \boldsymbol{P}_n\}$.

The derivative of W is calculated below,

$$\begin{aligned}\dot{W} &\le -\sum_{i=1}^{n}\left\{(\beta_i - 1)\|\boldsymbol{\xi}_i\|^2\right\} + \sum_{i=1}^{n}\Delta_i \le -(\beta - 1)\|\boldsymbol{\xi}_\Gamma\|^2 + \Delta \\ &\le -(\beta - 1)\lambda_{\max}^{-1}(\boldsymbol{P})W + \Delta\end{aligned} \tag{30}$$

where $\beta = \min\{\beta_i\}$, $\Delta = n\cdot\max\{\Delta_i\}$. $\lambda_{\max}(\boldsymbol{P})$ is the maximum eigenvalue of $\boldsymbol{P}$. By analogy with (16)~(17), for any constant $\delta > 0$, formulating a set $\Omega_\delta = \{\boldsymbol{\xi}_\Gamma \in R^{2n} | W \le \delta\}$, it is undoubtable that $\Omega_\delta \subset R^{2n}$. A sufficiently large β can be chosen to satisfy

$$\Delta \le 0.5(\beta - 1)\lambda_{\max}^{-1}(\boldsymbol{P})\delta. \tag{31}$$

Then substituting (31) into (30) results in

$$\dot{W} \le -(\beta - 1)\lambda_{\max}^{-1}(\boldsymbol{P})(W - 0.5\delta). \tag{32}$$

In what follows, it will be certified that, for any initial state $\boldsymbol{\xi}_\Gamma|_{t=0}$ confined in $\Omega = R^{2n}\backslash\Omega_\delta$, i.e., $W \ge \delta$, the trajectory of $\boldsymbol{\xi}_\Gamma$ will be unexceptionally captured by Ω_δ.

If this statement is not true, there must exist a finite time instant $t_f > 0$ such that $W|_{t=0} < W|_{t=tf}$ and $\dot{W}|_{t=tf} \ge 0$. But in the duration of $t \in [0, t_f)$, all components in $\boldsymbol{\xi}_\Gamma$ are well defined. $\dot{W}$ in (32) will always be a negative value, which results in the contradiction of $0 \le \dot{W}|_{t=tf} < 0$. Therefore, finite-time escaping phenomena would not occur, and $\boldsymbol{\xi}_\Gamma$ is uniformly bounded.

Step2: All the intermediate states can be practically regulated at the origin, and therefore, the global system large-signal stability is guaranteed.

For $\boldsymbol{\xi}_\Gamma \in \Omega$ and $W \ge \delta$, (32) can be further modified as

$$\dot{W} \le -0.5(\beta - 1)\lambda_{\max}^{-1}(\boldsymbol{P})\delta < 0. \tag{33}$$

It can be seen from (33) that, the DC MG which comprises DU subsystems has a Lyapunov function with a negative derivate, and hence, the MG is a stable system. Moreover, similar to the reasoning in Section III-B, β is inversely related to δ as suggested by (31). Given an invariant Δ, it is feasible to deliberately enlarge β such that δ nearly converges to zero. Hence, Ω_δ could be regulated to be arbitrarily small, and $\boldsymbol{\xi}_\Gamma$ is almost stabilized at the origin. As for the ith DU subsystems, z_{i1} z_{i2} and v_{Ci} will practically track the references z_{i1r}, z_{i2r} and v_{Cir}. In this sense, the output voltage controls of those subsystems have been realized. It is worth mentioning that, as observed from (22), reference values (v_{Cir} and z_{ir}) are only incorporated in the intermediate state calculations, and they do not involve the analyses from (27) to (33). Therefore, in

theory, the large-signal stability of the overall system would not be affected no matter whether MG is in CVM or DM.

IV. Discussions

A. Relationship Between DCC and CVM/DM

As mentioned earlier, either for CVM or DM, the two modes will always transmit the voltage references to the proposed DCC. The DCC then drives the DU output voltage to track the reference signal. When a DU is with CVM, the voltage reference would be a constant. In the case that the load power considerably increases, a single DU is no longer sufficient to feed all loads, and multiple DUs should be scheduled. They should be assigned with droop controllers to avoid voltage control conflicts. As in [24], the droop gain is defined as the ratio of the maximum bus voltage deviation over the maximum output power of a DU. Then all DUs would share the load in proportion to their ratings. In this sense, the DCC should harmoniously cooperate with CVM and DM to not only achieve the MG power management but also realize the large-signal stability of the whole system.

B. Relationship Between SSA and LSA

Generally, SSA is based on the linearized system model at a certain point; then the conventional transfer functions and bode plots can be utilized to identify the model stability. However, the SSA unfavorably presumes that the system merely experiences small-signal disturbances and there is only a slight deviation from the operating point. In contrast, the validity of LSA is not necessarily limited to operating point selections. When a system is stabilized in the large-signal sense, the system states would be invariantly brought to the designated values no matter how large/small the initial values of states are. Disregarding hardware limitations, in theory, it is possible to regulate the electrical system stabilizing at an arbitrarily designed point. Hence, the LSA validity holds in spite of equilibrium variations, whereas the SSA is only effective in the vicinity of an existing equilibrium. In this sense, the small-signal dynamics are certainly stable if MG large-signal stability is well accomplished.

C. Parameter Uncertainties in Canonical Modeling

For DUs in Fig. 2, the exact feedback linearization happens to provide the coordinate transformation that facilitates the boost converter canonical modeling. In fact, the proper coordinate transformations can be performed on other type of DC converters to obtain the corresponding canonical models. Afterward, the high gain observer and composite control law could be designed referring to (6) and (25). When it comes to parameter uncertainty issues, as indicated by [29], the uncertainties could be collectively embodied in the lumped disturbances that affect the stabilizations of all DU internal states, like (A5) in the Appendix. Then multiple observers should be applied to the differential equations of all transformed states, and the composite controller could be directly duplicated from (A12). Relevant large-signal stability analyses resemble the processes of Section III-D.

D. DC Load Dynamics

There are two types of loads in the DC system, i.e., resistive loads and constant power loads (CPLs). Those resistive loads are passive components which do not have their own dynamics, whereas CPLs usually refers to the power electronic loads whose consumed power is strictly regulated. Both resistive loads and CPLs absorb powers from the DC bus, while not contributing to establishing bus voltage. Alternatively, those DUs, including fuel cells, batteries and other distributed sources, would regulate the bus voltage. As long as DUs control the DC bus to accommodate various loads, then the DC system would be stable no matter how the loading condition varies. On the other hand, it is significant to pinpoint that the ideal CPL is the worst case since it has the negative incremental impedance in both low and high frequency bands, whereas the negative impedances of those converter based CPLs only appear in low frequency range. For the experimentations in Section VI, Chroma electronic load with up to 20kHz bandwidth could be viewed as an ideal CPL. It will show that the DCC is capable of handling the worst loading situation. The obtained conclusions that DCC is advantageous over the conventional PI, do stand, when less harsh loads (e.g., converter based CPLs) are coupled to the DC bus.

E. DC MG Aberrant Operations

DC MG aberrant operations can be classified into two types [30]. The first type refers to the failure that a DU converter fails to participate in DC bus voltage regulations because its output power reaches the upper limit. Then the DU power remains at the bounded value and the DU converts into the power control mode. In this case, for boost converters in Fig. 2, the reference should be slightly ameliorated, i.e., $-\hat{z}_{i12}$ in (20) should be displaced by the bounded power value. The second type pertains to the failures including switch faults, short-circuit and other mechanical dysfunctions. When DUs or loads encounter this type of fault, they have to disconnect from the main DC bus, thus preserving the rest parts of the system. Yet other DUs with DCC are still correctly functioning to stabilize the MG bus voltage.

F. Elusion of Non-Minimum Phase Issues

In (2), the capacitor voltage dynamic involves the control signal d_i. However, d_i is inversely related to the growth rate of v_{Ci}. If d_i slightly increases, the right-hand side of the second equation of (2) decreases, which slows down the growth rate of v_{Ci} and then causes a lesser increment of v_{Ci} during a certain time period. It is actually the inverse correlation of d_i and v_{Ci} growth rate that ultimately results in non-minimum phase issues, when intending to find a control input d_i to directly regulate the boost converter output voltage. However, after the coordinate transformation, in (6), the control input u_i linearly devotes to the growth rate of z_{i2}, and the increase of z_{i2} gives rise to the escalated z_{i1} growth rate. Therefore, no inverse relationship of u_i and the control output is found in the (6), and the boost converter canonical model is now exempted from the non-minimum phase problems.

V. Simulations

A. Parameters Tuning for the Boost Converter

Unlike the PI controllers that could be tuned in the frequency domain, the proposed DCC formulates the control law for DU converters straightly in the time domain. To select the relevant parameters of the high gain observer (10) and the composite controller (25), corresponding parameter tuning procedures will be provided in this section. Focusing on the ith DU in Fig. 2, no matter whether the DU works in CVM and DM, the output voltage reference is unexceptionally conveyed to the DCC who further forces v_{Ci} to track the desired value. For this reason, only CVM would be utilized for the parameter tuning, and the well-tuned quantities can be extended to DM without any change.

For the Hurwitz polynomial in (11), a characteristic function with multiple poles assigned as -1 can be formed below

$$(s+1)^3 = s^3 + 3s^2 + 3s + 1. \tag{34}$$

Matching the coefficients in (11) and (34) results in

$$l_{i1} = 3, l_{i2} = 3, l_{i3} = 1. \tag{35}$$

For the composite control law, k_{i1}, k_{i2} in equation (25) also subject to a Hurwitz polynomial

$$p_i(s) = s^2 + k_{i2}s + k_{i1}. \tag{36}$$

Similar to (34), a second-order characteristic function with repeated poles of -1 can be given as

$$(s+1)^2 = s^2 + 2s + 1. \tag{37}$$

By means of coefficient matching, k_{i1} and k_{i2} could be easily determined as 1 and 2 separately.

Then output power observing performances with different observer gains ($\sigma_i = 1000, 2000, 3000, 4000, 5000$) under dissimilar control gains ($\beta_i = 500, 750, 1000$), are shown in Fig. 4(a)$\sim$(c). It is apparent from Fig. 4(a) that the decreased σ_i leads to the slow observer dynamic. The tracking duration can be estimated as 1ms with σ_i of 5000, whereas the convergence time rises to 12ms when σ_i reduces to 1000. Comparing Fig. 4(a)$\sim$(c) reveals that performances of the high gain observer are little affected when β_i is differently set, which means the tuning of σ_i is almost decoupled from β_i variations. Proceeding to Fig. 4(d), output voltage transients are recorded under heterogeneous β_i settings (450, 550, 650, 850, 1000) while σ_i is fixed at 3000. The larger β_i causes the shorter voltage transition period. A long duration of about 15ms can be observed with β_i being selected as 450, whereas the voltage transient state accounts for only 6ms when $\beta_i = 1000$. Note that the high gain observer offers output power estimations for the state feedback control law, as in (22)$\sim$(25). The observer is supposed to bear faster dynamics than the control law. For instance, the settling times of the state feedback control law and the observer could be identified as 10ms and 2ms. The requirement, according to Fig. 4, can be satisfied by choosing σ_i and β_i as 3000 and 650 respectively. This set of parameters would be further utilized in the subsequent simulations and experimental verifications.

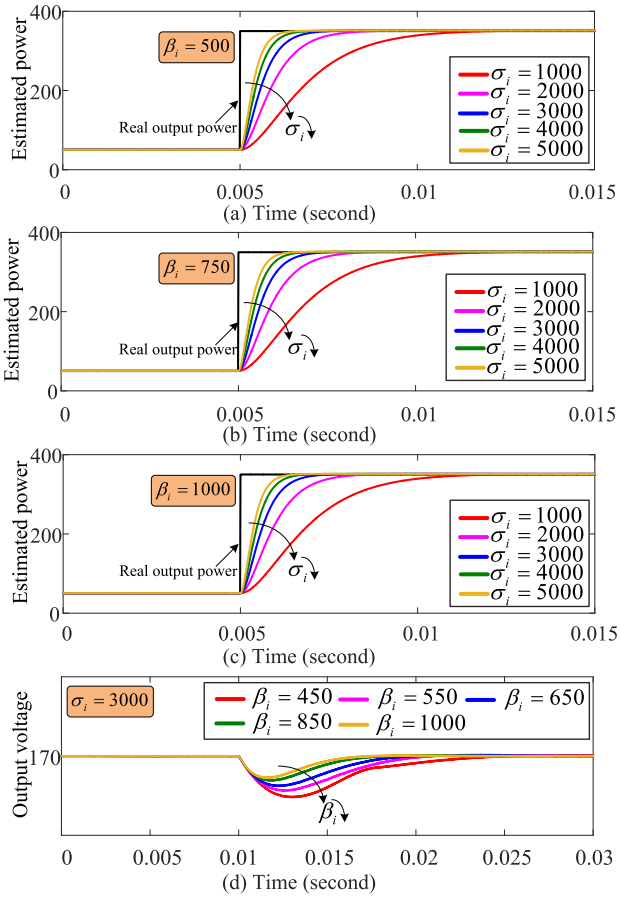

Fig. 4. Parameters tuning of σ_i and β_i. (a)-(c) Power estimations with σ_i variations when β_i is set as 500, 750 and 1000 respectively; (d) Transient voltage performances with β_i variations when σ_i is set as 3000.

TABLE II
System Parameters

Parameter	Description	Value
V^*	Nominal bus voltage	170V
L_1, L_2	Converter inductors	2mH
E_1, E_2	Input voltage	100V
C_1, C_2	Converter capacitors	470uF
f_{sw}	Switching frequency	20kHz
l_{11}, l_{12}, l_{13}	Observer gains for #1 converter	3, 3, 1
l_{21}, l_{22}, l_{23}	Observer gains for #2 converter	3, 3, 1
σ_1, σ_2	Observer scaling gains	3000
k_{11}, k_{12}	DCC parameters for #1 converter	1, 2
k_{21}, k_{22}	DCC parameters for #2 converter	1, 2
β_1, β_2	DCC scaling gains	650

B. Normal Operations Unifying CVM and DM

A DC system including two boost converters and the lumped load has been displayed in Fig. 5. System parameters are summarized in TABLE II. For Fig. 6, only converter#1 is utilized. It is working in CVM and the lumped load is a pure CPL. At the beginning, the CPL is configured as 50W. The inductor current and output power could be estimated as 0.5A and 50W. The bus voltage is stably regulated at 170V. When CPL surges to 350W at 0.05s, the estimated power (P_{o1_est}) given by the high gain observer quickly tracks the real output power in

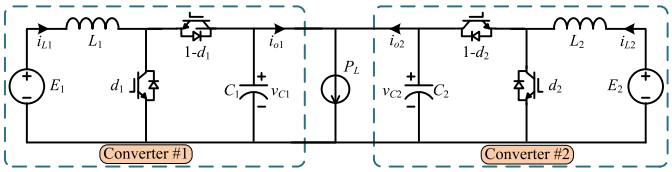

Fig. 5. Two boost converters feeding the lumped load P_L.

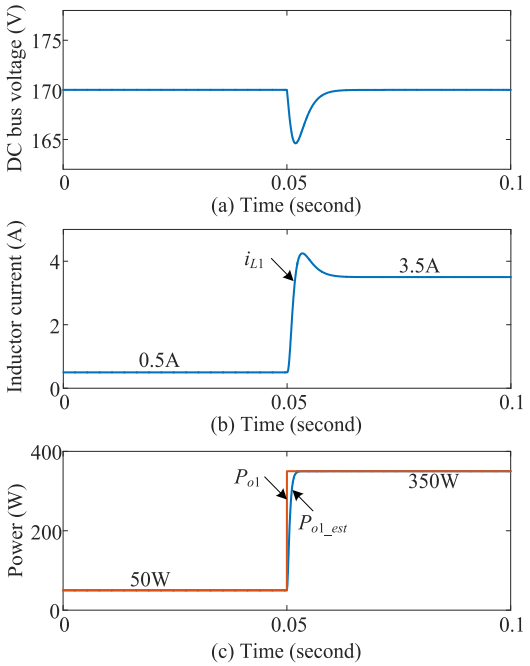

Fig. 6. Simulations for converter #1 in Fig.5 working in CVM.

a fast speed. The tracking duration could be approximated as 2ms, which is in good agreement with the parameter tuning results shown in Fig. 4 where the dynamics of observer and the composite control law are stipulated as 2ms and 10ms respectively. After the system transition, the DC bus voltage is recovered to 170V and the inductor current accordingly rises to 3.5A.

In Fig. 7, two boost converters are coordinately working in DM with droop gains being identically set as 0.01. This means the two converters should evenly share the load power in steady state. In the case that CPL is merely 100W, each converter is supposed to produce the power of 50W to load. Due to the droop mechanisms, the DC bus voltage would deviate from the nominal value (170V) and it is stabilized at 169.5V. i_{L1} and i_{L2} could be read as 0.5A. At 0.05s, CPL suddenly increases to 700W. The output powers of the two converters quickly grow to 350W. Similar to Fig. 6(c), the power values estimated by the high gain observers rapidly converge to the real powers in 2ms, as in Fig. 7(c) and (e). Responding to the enlarged CPL, the inductor currents rise to 3.5A in both boost converters.

C. Multi-Bus MG

To verify the effectiveness of the DCC in a more practical way, a representative multi-bus DC MG for controller testing is shown in Fig. 8. Without loss of generality, DU_1∼DU_4

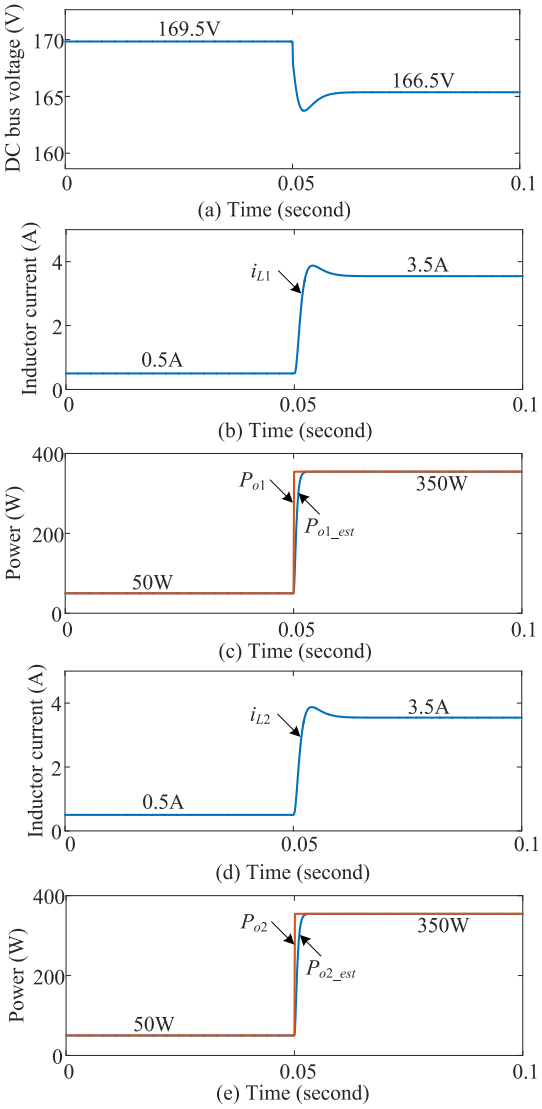

Fig. 7. Simulations for converters #1 and #2 in Fig.5 working in DM.

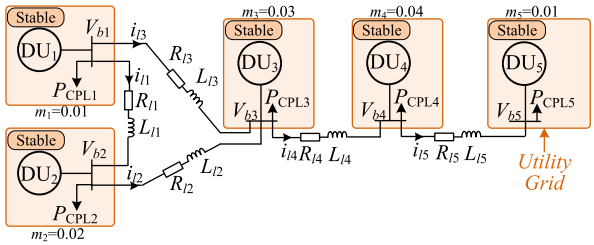

Fig. 8. A representative multi-bus DC MG.

are boost converter enabled DUs, whereas DU_5 represents the entity of an AC/DC rectifier and the utility grid. The modeling and DCC design for the rectifier have been elucidated in the Appendix. DU droop coefficients (m_1, m_2, m_3, m_4, m_5) are set as 0.01, 0.02, 0.03, 0.04 and 0.01 respectively. Relevant parameters including line resistances and line inductances are tabulated in TABLE III.

Notice that the proposed DCC basically provides an inner controller design that can drive the corresponding output voltage of a DU converter to track the reference generated either

TABLE III
SYSTEM PARAMETERS

Parameters	Values
R_{l1}, R_{l2}, R_{l3}, R_{l4}, R_{l5}	182mΩ
L_{l1}, L_{l2}, L_{l3}, L_{l4}, L_{l5}	39.4uH
m_1, m_2, m_3, m_4, m_5	0.01, 0.02, 0.03, 0.04, 0.01

TABLE IV
LOAD SCHEDULING FOR THE MULTI-BUS MG

	P_{CPL1}	P_{CPL2}	P_{CPL3}	P_{CPL4}	P_{CPL5}
0s	300W	0W	0W	0W	0W
1s	300W	0W→200W	0W	0W	0W
2s	300W	200W	0W→100W	0W	0W
3s	300W	200W	100W	0W→100W	0W
4s	300W	200W	100W	100W	0W→300W

from a droop controller (DM) or an invariant signal (CVM). It should be mentioned that, as highlighted in Fig. 8, each DU has its own DCC to stabilize the local bus and CPL in the large-signal sense. Thanks to the high gain observer, the DU converter systems are virtually decoupled from the DC network, and the local DC bus stabilities would be independent of cable line currents. In this regard, all buses can be viewed as stiff buses with droop features. From the aspect of connecting cable lines, they could only see the bus voltages established by DUs. Then differential equations delineating the cable line dynamics can be written as follows,

$$L_{l1}\dot{i}_{l1} = -R_{l1}i_{l1} + V_{b1} - V_{b2}, L_{l2}\dot{i}_{l2} = -R_{l2}i_{l2} + V_{b2} - V_{b3},$$
$$L_{l3}\dot{i}_{l3} = -R_{l3}i_{l3} + V_{b1} - V_{b3}, L_{l4}\dot{i}_{l4} = -R_{l4}i_{l4} + V_{b3} - V_{b4},$$
$$L_{l5}\dot{i}_{l5} = -R_{l5}i_{l5} + V_{b4} - V_{b5}. \quad (38)$$

Rearrange (38) into a compact form,

$$\dot{\boldsymbol{I}}_l = \boldsymbol{A}_l\boldsymbol{I}_l + \boldsymbol{B}_l\boldsymbol{V}_b, \quad (39)$$

where $\boldsymbol{I}_l = [i_{l1}\ i_{l2}\ i_{l3}\ i_{l4}\ i_{l5}]^T$, $\boldsymbol{A}_l = diag\{-R_{l1}/L_{l1}, -R_{l2}/L_{l2}, -R_{l3}/L_{l3}, -R_{l4}/L_{l4}, -R_{l5}/L_{l5}\}$ and $\boldsymbol{V}_b = [V_{b1}\ V_{b2}\ V_{b3}\ V_{b4}\ V_{b5}]^T$. $\boldsymbol{B}_l$ would be a bit complex and it can be written below,

$$\boldsymbol{B}_l = \begin{bmatrix} 1 & -1 & 0 & 0 & 0 \\ 0 & 1 & -1 & 0 & 0 \\ 1 & 0 & -1 & 0 & 0 \\ 0 & 0 & 1 & -1 & 0 \\ 0 & 0 & 0 & 1 & -1 \end{bmatrix}. \quad (40)$$

In (39), the signals in the input vector $\boldsymbol{V}_l$ are all rigorously stabilized. The stability of line network dynamics then relies on the eigenvalues of matrix $\boldsymbol{A}_l$. Noting that $\boldsymbol{A}_l$ is a diagonal matrix, the elements on its primary diagonal are de facto the matrix eigenvalues, i.e.,

$$p_1 = -\frac{R_{l1}}{L_{l1}}, p_2 = -\frac{R_{l2}}{L_{l2}}, p_3 = -\frac{R_{l3}}{L_{l3}}, p_4 = -\frac{R_{l4}}{L_{l4}}, p_5 = -\frac{R_{l5}}{L_{l5}}. \quad (41)$$

Substituting parameters in TABLE III into (41), eigenvalues are given as

$$p_1 = p_2 = p_3 = p_4 = p_5 = -4619.28, \quad (42)$$

which means the DC network constructed by the cables lines with *RL* impedances, is inherently a stable and passive system. As long as all DC buses are properly regulated, the MG is a stable system. In another world, the overall MG stability lies in the stabilization of each DC bus. For the proposed DCC, it synthesizes a high gain observer and a state feedback control law. The observer provides the estimations of the coupling of a DU system with other electrical devices. These estimations could be further offset by the feedback control law. By doing so, each DU is decoupled from the cable line based DC network and operates in an isolated way from the control and stability point of view. Note that the large-signal stabilization of the individual DU systems naturally leads to the stabilization of the respective DC bus in the large-signal sense. Together with the fact that cable line network is intrinsically stable and passive (see (42)), it is safe to conclude that the large-signal stability of the multi-bus DC MG in Fig. 8 has been perfectly accomplished by means of the proposed DCC.

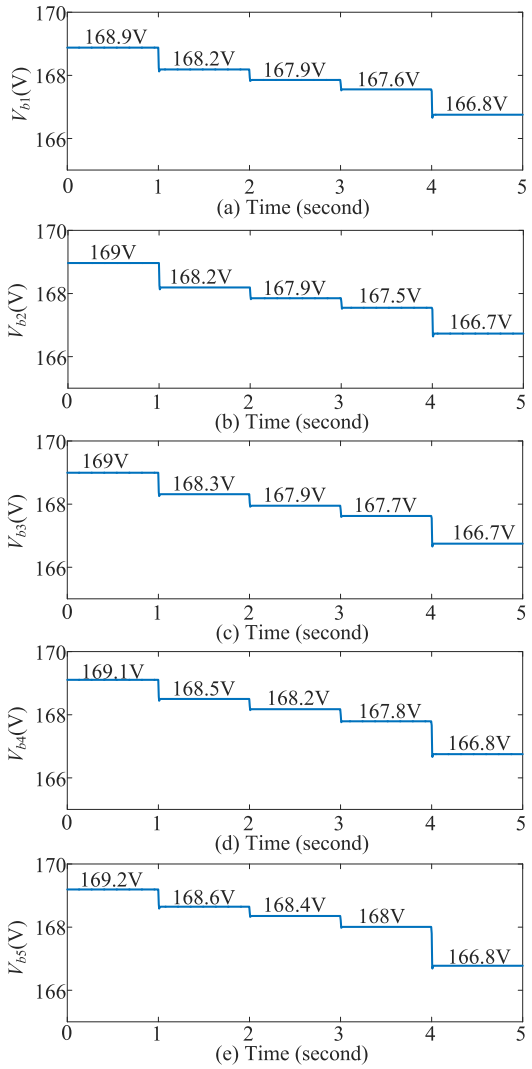

Fig. 9. Bus voltages in Fig. 8.

The supporting simulations are shown in Fig. 9. and Fig. 10. The scheduling of load powers has been recorded in TABLE IV. In the beginning, P_{CPL1} is set as 300W whereas

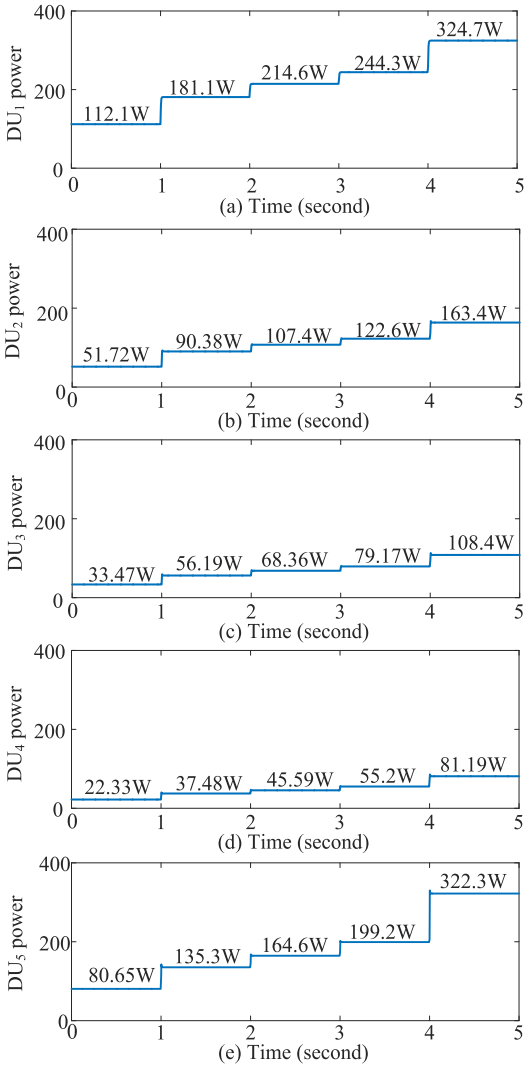

Fig. 10. DU powers in Fig. 8.

other CPLs are not configured. From Fig. 9, the five bus voltages could be read as 168.9V, 169V, 169V, 169.1V and 169.2V respectively. The output powers of the five DUs are 112.1W, 51.72W, 33.47W, 22.33W and 80.65W. Once the CPL at bus2 (V_{b2}) increases to 200W, the voltage drops at all buses are estimated as 0.7V (see Fig. 9.), and DU powers are recorded as 181.1W, 90.38W, 56.19W, 37.48W and 135.3W separately. At the instants of 2s, 3s and 4s, P_{CPL3}, P_{CPL4} and P_{CPL5} are enabled in sequence, as detailed in TABLE IV. The bus voltages continuously step down, and they are roughly identical at 166.7V when all loads are activated. Accordingly, the DU output powers sequentially step up. In the case of full load (4∼5s), the DU powers are measured as 324.7W, 163.4W, 108.4W, 81.19W and 322.3W respectively. It should be noted that, based on droop control mechanisms, the ideal power sharing ratio of the five DUs can be calculated as 12: 6: 4: 3: 12. Overviewing the testing process in Fig. 9 and Fig. 10, although the power ratio is not exactly consistent with the expected quantity, all DUs make efforts to supply powers to all MG loads, which is acceptable in practical engineering.

TABLE V
CVM TESTS (ONLY CONVERTER#1 USED)

	Voltage reference	Load
Case 1	v_{C1r}:170V	CPL: 50W→350W;
Case 2	v_{C1r}:170V→160V; v_{C1r}:170V→150V;	CPL: 550W;
Case 3	v_{C1r}:170V	CPL: 50W→650W;

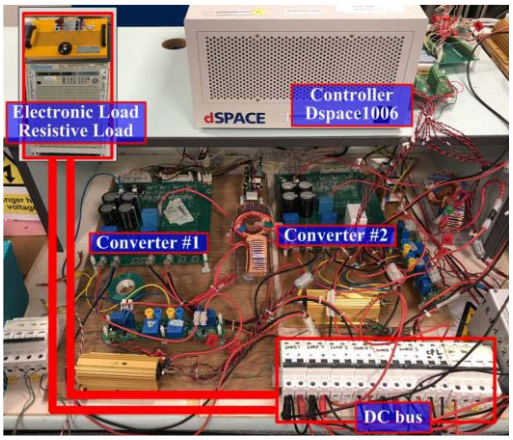

Fig. 11. Experimental setup.

VI. EXPERIMENTAL VERIFICATIONS

To corroborate the effectiveness and feasibility of the DCC, an in-house experimental platform is built up, as displayed in Fig. 11. The one-line diagram has been given in Fig. 5. The platform consists of a Dspace 1006 controller, two boost converters, the lumped load (a resistive load and an electronic load). Related parameters are the same in simulations (see Table II). The inductances and capacitances are chosen as 2mH and 470uF, according to the design guideline in [26]. There are two small resistors of 0.2Ω installed between converter terminals and DC bus to avoid the rush current induced by the difference of terminal capacitors. As mentioned earlier, resistive loads and CPSs would not deteriorate the MG stability. The most challenging case is that the lumped load is a pure CPL. In this section, the electronic load acting as a CPL is integrated to the DC bus, and for operating safety, the resistive load is also incorporated into the system. It should be noted that the damping effect devoted by the resistor is minor because the resistance is purposely tuned to be excessively large, i.e., 1698Ω. Hence, the CPL still overwhelmingly dominates the lumped load. On these bases, as in TABLE V and TABLE VI, 6 cases are arranged to compare the voltage control performances of the converters under the DCC and the PI. Experimental results will show that the former method helps to stabilize the DC MG and contributes larger operation range than the latter one in both CVM and DM.

A. CVM (Constant Voltage Mode)

1) Case 1: This case investigates regular system operations in CVM. The key parameters in the DCC have been provided in TABLE II. PI parameters (voltage loop: $k_p = 0.1$,

TABLE VI
DM TESTS (BOTH TWO CONVERTERS USED)

	Droop Coefficient	Load
Case 4	m_1=m_2=0.01;	CPL: 100W→700W;
Case 5	m_1=m_2=0.02; m_1=m_2=0.04;	CPL:100W→700W;
Case 6	m_1=m_2=0.01;	CPL:100W→1000W;

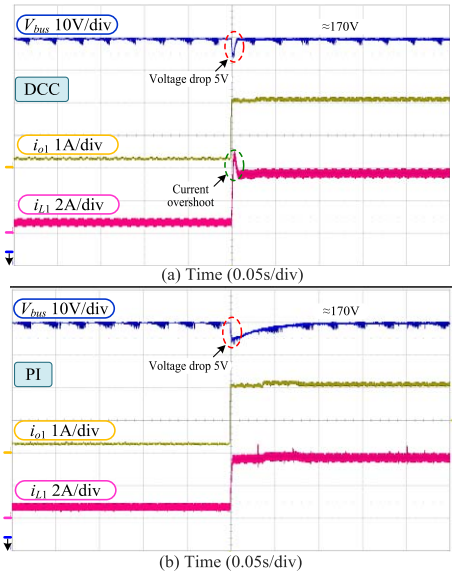

Fig. 12. Case 1: CVM with CPL from 50W to 350W.

k_i = 15.75; current loop: k_p = 0.775, k_i = 24.35;) are selected complying to the design standards reported in [27]. The parameters are further adjusted slightly so that voltage deviations resulted from load changes are identical to that with the DCC. Hence, it is fair to conduct the necessary comparisons of DCC and PI controllers.

As shown in Fig. 12, DC bus is rigorously regulated at 170V at the beginning. When a sudden CPL step-up from 50W to 350W is activated, identical voltage drops (5V) are observed for both PI and DCC controls. It is conspicuous that the DCC is competent to restore the bus voltage to its nominal value (170V) within about 10ms, whereas the voltage recovery time of PI is estimated as 70ms. A slight overshoot on the inductor current i_{L1} (see Fig. 12(a)) is due to the fact that the DCC endeavors to transfer more power from the source to the load for shortening the transient duration. Hence, the load-changing effects on the bus voltage can be minimized.

2) Case 2: As understood from [31], a DC system integrated with an invariant CPL and a resistor may suffer from more serious stability problems when the bus voltage is lowered. Motivated by this assertion, different from case 1 where MG voltage is maintained strictly at 170V, case 2 examines the system stability given that the voltage reference declines while the CPL maintains at a comparatively high level (550W). As shown in Fig. 13, when v_{C1r} steps down from 170V to 160V, the MG is stable under both DCC and PI controls. However, transient oscillations of the bus voltage and the inductor current are found in the PI regulated system. In the situation that

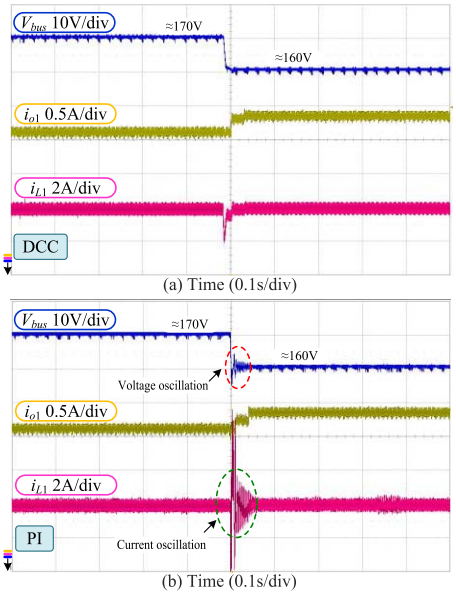

Fig. 13. Case 2: CVM with v_{C1r} from 170V to 160V.

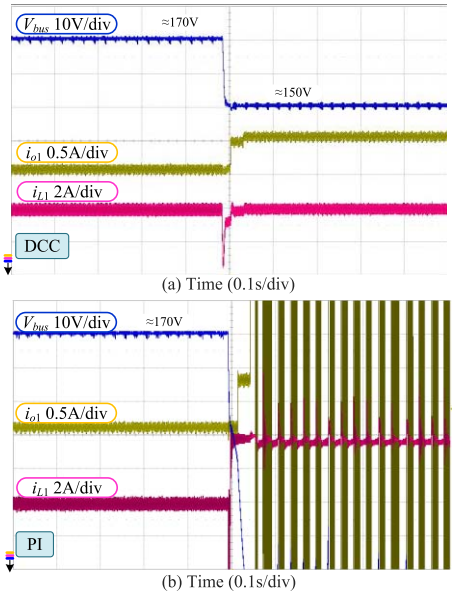

Fig. 14. Case 2: CVM with v_{C1r} from 170V to 150V.

v_{C1r} reduces from 170V to 150V, as recorded in Fig. 14, the system with the PI unfortunately collapses, whereas the DCC stabilizes the DC bus voltage at the targeted value.

3) Case 3: Following case 1, case 3 studies a scenario that the CPL abruptly surges from 50W to 650W, and experimental results have been shown in Fig. 15. For this atrocious case, with the proposed DCC, although a voltage drop of 10V occurs at the instant of a load change, the bus voltage quickly recovers to 170V in a short time, which means voltage regulation has been realized. In contrast, the PI controller fails to survive this huge CPL increase, and the entire MG system is destabilized.

Summarily, the results in case 2 and case 3 experimentally consolidates the theoretical analyses of Section III-D that, the DCC can extend the system operating margin and attain the

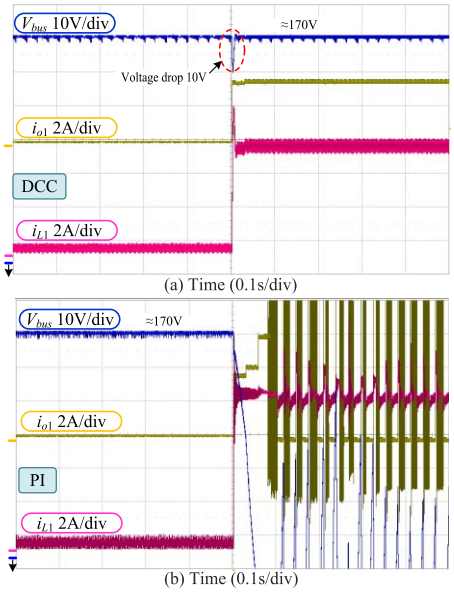

Fig. 15. Case 3: CVM with CPL from 50W to 650W.

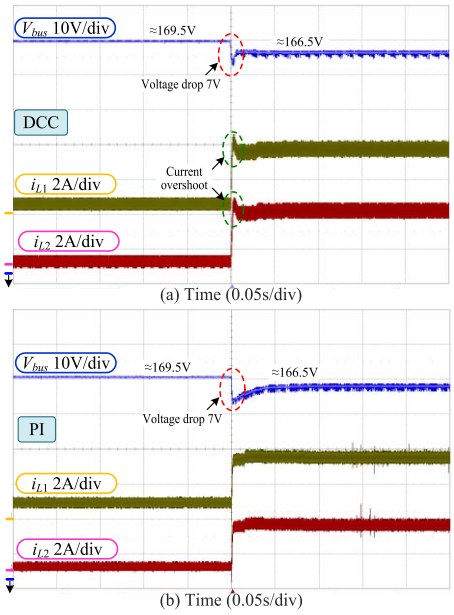

Fig. 16. Case 4: DM with $m_1 = m_2 = 0.01$ and CPL from 100W to 700W.

large-signal stability. By using DCC, considerable equilibrium changes are permitted by the MG, and thus, operation flexibility can be markedly raised. Besides, for the lab setup, the nominal power of the DU boost converter is 560W with the design margin of 20%. In case 3, the CPL with 650W has already exceeded the nominal value, which means the DCC still works elegantly even in overloading condition.

B. DM (Droop Mode)

1) Case 4: Fig. 16 shows experimental results with the droop coefficients of two converters set as 0.01 when the CPL steps up from 100W to 700W. In this case, DU would evenly share CPL variations. For DCC and PI controls, they respond

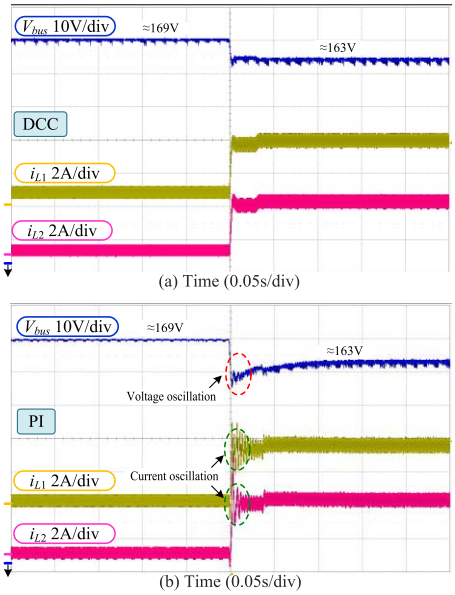

Fig. 17. Case 5: DM with $m_1 = m_2 = 0.02$ and CPL 100W to 700W.

to the identical droop controller. The same voltage drops of around 7V are observed when the load increase is triggered. The DC bus reaches a new level which is 166.5V. Differences lie in that the DCC spends 10ms on the bus voltage transition, whereas the PI controller takes estimated 50ms. Similar to case 1, inductor overshoots are found during system transitions by employing the DCC. These phenomena could be well explained by exigent power transfer enforced by the DCC from the source to the load. As a result, more rapid system dynamics can be acquired.

2) Case 5: It is important to reiterate that droop controllers intentionally enlarge the output impedances of the converters, which is a compromised solution to sidestep the voltage conflictions of multiple sources. The increased droop gains may induce more power interactions between CPL and sources [6], thus possibly aggravating the MG stability. For this reason, different from ordinary operations shown by case 4, case 5 would explore the impacts of droop gain fluctuations on the MG performances.

With reference to TABLE VI, droop gains are chosen as 0.02 for the two converters at first. The bus voltage fixes at 169V when the CPL is scheduled as 100W (see Fig. 17). When the CPL unexpectedly rises to 700W, both DCC and PI controls can stably regulate the bus voltage at around 163V. It should be noted that the PI controller causes transient voltage and current oscillations, while the proposed DCC allows a smoother system transition. Continuing to increase the droop gains to 0.04, relevant results have been shown in Fig. 18. The PI controller based MG is unstable under the CPL step-up, whereas the DCC regulates the bus voltage stabilized at a new value that is 156V.

3) Case 6: Subsequent to case 4, in this case, droop gains are maintained invariant as 0.01. The overall system stabilities regulated by both DCC and PI controllers are compared when the CPL brutally grows to 1000W. As plotted in Fig. 19(a),

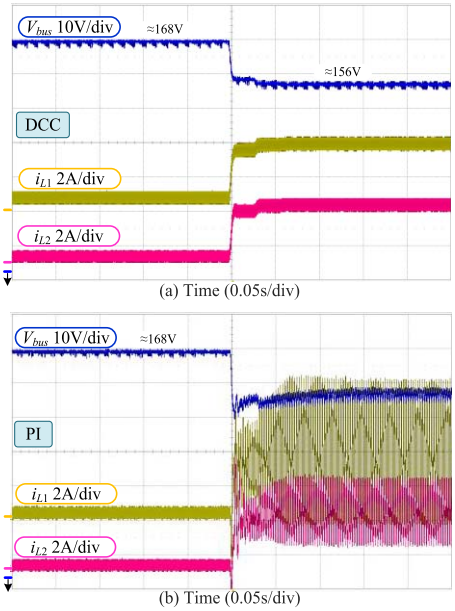

Fig. 18. Case 5: DM with $m_1 = m_2 = 0.04$ and CPL 100W to 700W.

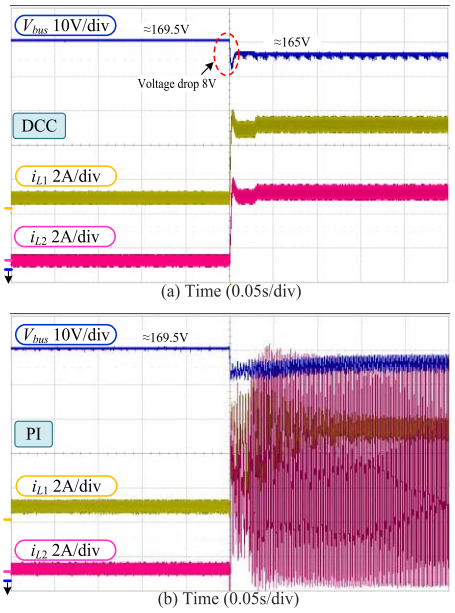

Fig. 19. Case 6: DM with $m_1 = m_2 = 0.01$ and CPL 100W to 1000W.

although voltage drop of 8V is inspected in the transient state, the DCC stabilizes the DC bus at 165V after the CPL step-up is enabled. Unluckily, this cruel load increase cannot be tolerated under the PI control case, and thus, the whole MG is unstable, as depicted in Fig. 19(b).

Conclusively, the observations reported by case 5 and case 6 again validate that the DCC proposed in this paper is a large-signal stabilizer. It can weather large system disturbances and ensures stable operations in a wider range.

From the six cases in this section, the DCC prevails over the PI control in terms of faster bus voltage transition and wider system operating range. Although the PI may engender the overshoot/drop of current/voltage being within allowable limit, the PI control has its inherent disadvantages such as neglecting parts of dynamics when establishing DU models and failing to address the fiendish coupling effects among DUs. Differently, the observer synthesized in the DCC helps to rapidly and accurately estimate the couplings which are further involved in the composite control law. This maneuver decouples a particular DU from neighboring devices, from the perspective of control and stability. Moreover, the DCC ensures the negative derivative of each DU Lyapunov function, thus resulting in the large-signal stability. By adopting DCC, no system dynamics are overlooked, and the large-signal stability holds no matter how far the initial values of the DU internal state are away from the expected ones.

VII. Conclusion

In this paper, a novel DCC is proposed to serve as a large-signal stabilizer for a DC MG system. For a certain subsystem, the electrical coupling imposed by the externals in the MG can be estimated by a properly designed high gain observer. Then the coupling can be counteracted by the DCC, which enables the DU subsystem to virtually work in a separated manner. On these bases, the stabilization task of the whole MG system could be dissembled into the stabilizations of single subsystems. Specifically, the global system large-signal stability would be attained as long as the internal states inside each DU subsystems are appositely stabilized. Therefore, the proposed controller is decentralized, which escalates the MG flexibility, reliability and PnP functionality to a large measure. Besides, by using the DCC, the compromises between system model completeness and LSA can be elegantly shunned. Related theoretical analyses based on Lyapunov functions are also provided. Comparative studies performed on a hardware platform demonstrate that the DCC takes advantages over the traditional PI by shortening the MG transition duration and broadening the system stability margin.

Appendix

As in Section III, with DCC, MG system large-signal stabilization can be realized by only guaranteeing the individual converter large-signal stability. This means the DCC could be separately formulated for each single DU. The DCC design for a given DU converter includes three steps which are the canonical DU modeling, the high gain observer design and the composite controller design. It should be mentioned that the aforesaid first step is of high importance. DU converters in the MG could be uniformly written into the canonical forms like (6) through proper coordinate transformations. Then, all DUs have similar mathematical expressions, which permits the DCCs that already work well with the existing DUs being easily generalized to a new DU member. For both CVM and DM, two modes generate voltage references to the DCC that would regulate the real output voltage to track the desired value. Given the need of conciseness, while not compromising generality, in this section, DCC design procedures are applied to buck converter, buck-boost converters and AC/DC rectifier working in CVM. If these DU converters intend to work in

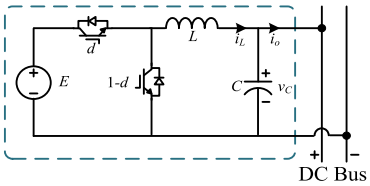

Fig. A1. Schematic of a buck converter.

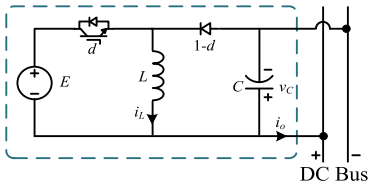

Fig. A2. Schematic of a buck-boost converter.

DM, one may simply change the voltage reference generating pattern, while DCC controllers remain unaffected at all.

A. Buck Converter

The schematic of a buck converter linked to a DC bus is shown in Fig. 1. The dynamic equations regarding the inductor current i_L and capacitor voltage v_C could be written below,

$$L\dot{i}_L = Ed - v_C, C\dot{v}_C = i_L - i_o, \tag{A1}$$

where E, d, L, C and i_o are input voltage, duty cycle, inductance, capacitance and output current. Then the DCC could be obtained by following the preceding three designing steps.

1) Canonical DU Modeling: The first internal state z_1 in the buck converter can be expressed as $z_1 = 0.5Cv_C^2$. Taking the time derivative of z_1 gives

$$\dot{z}_1 = Cv_C\dot{v}_C = Cv_C\left(\frac{i_L - i_o}{C}\right) = v_Ci_L + \varsigma_1, \varsigma_1 = -v_Ci_o. \tag{A2}$$

Observing (A2), v_Ci_L could be defined as the second internal state z_2 whose time derivative is

$$\dot{z}_2 = v_C\dot{i}_L + i_L\dot{v}_C = v_C\left(\frac{Ed - v_C}{L}\right) + i_L\left(\frac{i_L - i_o}{C}\right) = u + \varsigma_2$$
$$u = \frac{v_CEd}{L} - \frac{v_C^2}{L} + \frac{i_L^2}{C}, \varsigma_2 = -\frac{i_Li_o}{C}, \tag{A3}$$

where u is the equivalent control input, and the duty cycle could be computed as the following,

$$d = \left(u + \frac{v_C^2}{L} - \frac{i_L^2}{C}\right)\frac{L}{Ev_C}. \tag{A4}$$

Slightly manipulating (A2) and (A3) results in the canonical form of the buck converter,

$$\dot{z}_1 = z_2 + \varsigma_1, \dot{z}_2 = u + \varsigma_2. \tag{A5}$$

2) High Gain Observer Design: In (A5), ς_1 and ς_2 are the disturbance terms that impact the dynamic states z_1 and z_2. Both these disturbances, as elaborated previously, can be regarded as the electrical coupling of buck converter with other devices. Resembling (10), the high gain observers can be designed to estimate the necessary information of ς_1 and ς_2 respectively.

$$\begin{cases} \dot{\hat{z}}_{11} = z_2 + \hat{z}_{12} + l_{11}\sigma(z_1 - \hat{z}_{11}) \\ \dot{\hat{z}}_{12} = \hat{z}_{13} + l_{12}\sigma^2(z_1 - \hat{z}_{11}) \\ \dot{\hat{z}}_{13} = l_{13}\sigma^3(z_1 - \hat{z}_{11}) \end{cases}, \tag{A6}$$

$$\begin{cases} \dot{\hat{z}}_{21} = u + \hat{z}_{22} + l_{21}\sigma(z_2 - \hat{z}_{21}) \\ \dot{\hat{z}}_{22} = l_{22}\sigma^2(z1 - \hat{z}_{21}) \end{cases}, \tag{A7}$$

where $\hat{z}_{11}, \hat{z}_{12}, \hat{z}_{13}$ are the estimates of z_1, ς_1, $\dot{\varsigma}_1$. $\hat{z}_{21}, \hat{z}_{22}$ are the estimates of z_2, ς_2. $\sigma > 1$ is a positive scaling gain. Col(l_{11}, l_{12}, l_{13}) and Col(l_{21}, l_{22}) are observer gain vectors with their components being the coefficients of Hurwitz polynomials. The convergence and stability analyses of the observers in (A6) and (A7) has been exhibited in (11)∼(19), and they are not planned here to avoid unnecessary duplications.

3) Composite Controller Design: The couplings estimated above should be countervailed by the proposed DCC. To this end, referring to (22), intermediate states could be declared first,

$$\xi_1 = z_1 - z_{1r}, \xi_2 = (z_2 - z_{2r})/\beta, v = (u - u_r)/\beta^2 \tag{A8}$$

where $\beta > 1$ is a positive scaling gain. v is an auxiliary control input. z_{1r}, z_{2r} and u_r denote the reference signals for z_1, z_2 and u; they can be recursively computed by manipulating (A5)∼(A7),

$$z_{1r} = 0.5Cv_{Cr}^2, z_{2r} = \dot{z}_{1r} - \hat{z}_{12}, u_r = \ddot{z}_{1r} - \hat{z}_{13} - \hat{z}_{22}. \tag{A9}$$

v_{Cr} is the output voltage reference. It is vital to note that, in (A8), buck converter internal states (z_1, z_2) and control input u will approximate to the respective references if the intermediate states are regulated to zeros. Then the output voltage control for the buck converter is achieved. Taking the differentiation of ξ_1 and ξ_2 leads to the following dynamic equations,

$$\dot{\xi}_1 = \beta\xi_2 + \sigma e_{12}, \dot{\xi}_2 = \beta v + l_{12}\sigma^2 e_{11}/\beta + \sigma e_{22}/\beta. \tag{A10}$$

To stabilize the above states, a linear state feedback control law that contains both ξ_1 and ξ_2 can be designed,

$$v = -k_1\xi_1 - k_2\xi_2. \tag{A11}$$

k_1 and k_2 correspond to the Hurwitz polynomial coefficients. Then the equivalent control u could be identified as

$$u = -\beta^2(k_1\xi_1 + k_2\xi_2) + u_r. \tag{A12}$$

For the close loop system governed by (A10)∼(A12), its large-signal stability is similar to the process in (27)∼(33) disregarding the subscript "i" in pertinent equations.

B. Buck-Boost Converter

With regard to the buck-boost converter displayed in Fig. 2, the average model can be given as

$$L\dot{i}_L = dE - (1 - d)v_C, C\dot{v}_C = (1 - d)i_L - i_o. \tag{A13}$$

A coordinate transformation could be performed on (A13),

$$z_1 = \frac{1}{2}Li_L^2 + \frac{1}{2}Cv_C^2 + CEv_C, z_2 = Ei_L. \tag{A14}$$

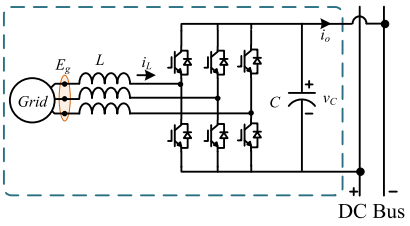

Fig. A3. Schematic of an AC/DC rectifier.

Compute the time derivatives of z_1 and z_2 individually,

$$\begin{aligned}\dot{z}_1 &= Li_L\dot{i}_L + Cv_C\dot{v}_C + CE\dot{v}_C \\ &= Li_L\left(\frac{dE}{L} - \frac{1-d}{L}v_C\right) + Cv_C\left(\frac{1-d}{C}i_L - \frac{i_o}{C}\right) \\ &\quad + CE\left(\frac{1-d}{C}i_L - \frac{i_o}{C}\right) \\ &= Ei_L - (E+v_C)i_o \\ \dot{z}_2 &= E\dot{i}_L = \frac{E^2}{L}d - \frac{(1-d)Ev_C}{L} = u. \end{aligned} \tag{A15}$$

Manipulate (A15) into the canonical model,

$$\begin{cases}\dot{z}_1 = z_2 + \varsigma \\ \dot{z}_2 = u\end{cases} \tag{A16}$$

where $\varsigma = -(E + v_C)i_o$ is the disturbance. The relation between d and u can thus be quantified as

$$d = \frac{Lu + Ev_C}{E^2 + Ev_C}. \tag{A17}$$

Inspecting (A16), it now has the identical form to the boost converter canonical model as in (6). In this sense, the high gain observer (10) and the composite controller (25) can be directly extended to (A16) without any change. Then the large-signal stabilization of the buck-boost converter will be spontaneously attained.

C. AC/DC Rectifier

As comprehended in [27], the mathematical model of an AC/DC rectifier in Fig. 3 can be expressed in the rotating frame,

$$\begin{aligned}L\dot{i}_{Ld} &= L\omega i_{Lq} + E_{gd} - v_C S_d \\ L\dot{i}_{Lq} &= -L\omega i_{Ld} - v_C S_q \\ C\dot{v}_C &= \frac{3}{2}\frac{E_{gd}i_{Ld}}{v_C} - i_o. \end{aligned} \tag{A18}$$

where L and $C$are inductance and capacitance. ω denotes the grid angular frequency. i_{Ld} and i_{Lq} represent the inductor currents after dq transformation. v_C is the output capacitor voltage. Assuming that the AC/DC converter is operating in unit power factor, in dq frame, the d-axis component E_{gd} of the grid voltage is also the grid amplitude, while the voltage component in q-axis is zero. i_o is output current. S_d and S_q are switch functions which are the control inputs.

To obtain a canonical model similar to (6), a new state z_1 can be formulated as

$$z_1 = 0.5Cv_C^2. \tag{A19}$$

Computing the derivative of z_1 gives

$$\dot{z}_1 = Cv_C\left(\frac{3E_{gd}i_{Ld}}{2Cv_C} - \frac{i_o}{C}\right) = \frac{3}{2}E_{gd}i_{Ld} + \varsigma \tag{A20}$$

where $\varsigma = -v_C i_o = -P_o$ is the disturbance term that may affect the stabilization of z_1. The second state z_2 could be selected as $3/2E_{gd}i_{Ld}$, and its derivative is

$$\dot{z}_2 = \frac{3}{2}E_{gd}\left(\omega i_{Lq} + \frac{E_{gd}}{L} - \frac{v_C}{L}S_d\right) = u. \tag{A21}$$

Combining (A20) and (A21), new dynamics can be obtained,

$$\dot{z}_1 = z_2 + \varsigma, \dot{z}_2 = u, \tag{A22}$$

where u is the equivalent control input. The relationship between u and S_d can be determined below,

$$S_d = \frac{E_{gd}/L + \omega i_{Lq} - 2u/\left(3E_{gd}\right)}{v_C/L}. \tag{A23}$$

Note that (A22) for the AC/DC rectifier model is in identical format to (6). Similar to the situation in the buck-boost converter, it is possible to apply the high gain observer (10) and the composite controller (25) to (A22), and the transformed internal states z_1, z_2 would be satisfactorily stabilized in the large-signal sense. As for the second dynamic equation in (A18), it is a first-order equation and i_{Lq} should be regulated to zero in steady state for unit power factor operation. Therefore, S_q could be easily written as

$$S_q = \left(k_q i_{Lq} - \omega i_{Ld}\right)\frac{L}{v_C} \tag{A24}$$

where k_q is a positive constant. Substituting (A24) to the second dynamic equation into (A18) yields,

$$\dot{i}_{Lq} = -k_q i_{Lq}, \tag{A25}$$

which suggests i_{Lq} is asymptotically stable and would decay to zero in steady state.

REFERENCES

[1] G. F. Reed, "DC technologies: Solutions to electric power system advancements [Guest Editorial]," *IEEE Power Energy Mag.*, vol. 10, no. 6, pp. 10–17, Nov./Dec. 2012.

[2] H. Liu *et al.*, "An enhanced dual droop control scheme for resilient active power sharing among paralleled two-stage converters," *IEEE Trans. Power Electron.*, vol. 32, no. 8, pp. 6091–6104, Aug. 2017.

[3] M. Su, Z. Liu, Y. Sun, H. Han, and X. Hou, "Stability analysis and stabilization methods of DC microgrid with multiple parallel-connected DC–DC converters loaded by CPLs," *IEEE Trans. Smart Grid*, vol. 9, no. 1, pp. 132–142, Jan. 2018.

[4] J. Xiao, P. Wang, and L. Setyawan, "Implementation of multiple-slack-terminal DC microgrids for smooth transitions between grid-tied and Islanded states," *IEEE Trans. Smart Grid*, vol. 7, no. 1, pp. 273–281, Jan. 2016.

[5] M. Wu and D. D.-C. Lu, "A novel stabilization method of LC input filter with constant power loads without load performance compromise in DC microgrids," *IEEE Trans. Ind. Electron.*, vol. 62, no. 7, pp. 4552–4562, Jul. 2015.

[6] A. P. N. Tahim, D. J. Pagano, E. Lenz, and V. Stramosk, "Modeling and stability analysis of Islanded DC microgrids under droop control," *IEEE Trans. Power Electron.*, vol. 30, no. 8, pp. 4597–4607, Aug. 2015.

[7] Q. Xu, P. Wang, J. Chen, C. Wen, and M. Y. Lee, "A module-based approach for stability analysis of complex more-electric aircraft power system," *IEEE Trans. Transport. Electrific.*, vol. 3, no. 4, pp. 901–919, Dec. 2017.

[8] F. Gao, X. Zheng, S. Bozhko, C. I. Hill, and G. Asher, "Modal analysis of a PMSG-based DC electrical power system in the more electric aircraft using eigenvalues sensitivity," *IEEE Trans. Transport. Electrific.*, vol. 1, no. 1, pp. 65–76, Jun. 2015.
[9] L. Guo *et al.*, "Stability analysis and damping enhancement based on frequency-dependent virtual impedance for DC microgrids," *IEEE J. Emerg. Sel. Topics Power Electron.*, vol. 5, no. 1, pp. 338–350, Mar. 2017.
[10] M. Hamzeh, M. Ghafouri, H. Karimi, K. Sheshyekani, and J. M. Guerrero, "Power oscillations damping in DC microgrids," *IEEE Trans. Energy Convers.*, vol. 31, no. 3, pp. 970–980, Sep. 2016.
[11] M. A. Kardan *et al.*, "Improved stabilization of nonlinear DC microgrids: Cubature Kalman filter approach," *IEEE Trans. Ind. Appl.*, vol. 54, no. 5, pp. 5104–5112, Sep./Oct. 2018.
[12] Z. Liu *et al.*, "Existence and stability of equilibrium of DC microgrid with constant power loads," *IEEE Trans. Power Syst.*, to be published, doi: 10.1109/TPWRS.2018.2849974.
[13] Y. Gu, W. Li, and X. He, "Passivity-based control of DC microgrid for self-disciplined stabilization," *IEEE Trans. Power Syst.*, vol. 30, no. 5, pp. 2623–2632, Sep. 2015.
[14] J. Yu *et al.*, "Passivity-based active stabilization for DC microgrid applications," *CSEE J. Power Energy Syst.*, vol. 4, no. 1, pp. 29–38, Mar. 2018.
[15] S. Sanchez and M. Molinas, "Large signal stability analysis at the common coupling point of a DC microgrid: A grid impedance estimation approach based on a recursive method," *IEEE Trans. Energy Convers.*, vol. 30, no. 1, pp. 122–131, Mar. 2015.
[16] P. Magne, D. Marx, B. Nahid-Mobarakeh, and S. Pierfederici, "Large-signal stabilization of a DC-link supplying a constant power load using a virtual capacitor: Impact on the domain of attraction," *IEEE Trans. Ind. Appl.*, vol. 48, no. 3, pp. 878–887, May/Jun. 2012.
[17] A. Houari *et al.*, "Large-signal stabilization of AC grid supplying voltage-source converters with LCL-filters," *IEEE Trans. Ind. Appl.*, vol. 51, no. 1, pp. 702–711, Jan./Feb. 2015.
[18] M. N. Hussain, R. Mishra, and V. Agarwal, "A frequency-dependent virtual impedance for voltage-regulating converters feeding constant power loads in a DC microgrid," *IEEE Trans. Ind. Appl.*, vol. 54, no. 6, pp. 5630–5639, Nov./Dec. 2018.
[19] H. R. Baghaee, M. Mirsalim, and G. B. Gharehpetian, "Performance improvement of multi-DER microgrid for small- and large-signal disturbances and nonlinear loads: Novel complementary control loop and fuzzy controller in a hierarchical droop-based control scheme," *IEEE Syst. J.*, vol. 12, no. 1, pp. 444–451, Mar. 2018.
[20] H. R. Baghaee, M. Mirsalim, G. B. Gharehpetian, and H. A. Talebi, "A decentralized robust mixed H2/H∞ voltage control scheme to improve small/large-signal stability and FRT capability of Islanded multi-DER microgrid considering load disturbances," *IEEE Syst. J.*, vol. 12, no. 3, pp. 2610–2621, Sep. 2018.
[21] M. Kabalan, P. Singh, and D. Niebur, "Large signal Lyapunov-based stability studies in microgrids: A review," *IEEE Trans. Smart Grid*, vol. 8, no. 5, pp. 2287–2295, Sep. 2017.
[22] D. Marx, P. Magne, B. Nahid-Mobarakeh, S. Pierfederici, and B. Davat, "Large signal stability analysis tools in DC power systems with constant power loads and variable power loads—A review," *IEEE Trans. Power Electron.*, vol. 27, no. 4, pp. 1773–1787, Apr. 2012.
[23] T. Dragičević, J. M. Guerrero, J. C. Vasquez, and D. Škrlec, "Supervisory control of an adaptive-droop regulated DC microgrid with battery management capability," *IEEE Trans. Power Electron.*, vol. 29, no. 2, pp. 695–706, Feb. 2014.
[24] P. Lin *et al.*, "An integral droop for transient power allocation and output impedance shaping of hybrid energy storage system in DC microgrid," *IEEE Trans. Power Electron.*, vol. 33, no. 7, pp. 6262–6277, Jul. 2018.
[25] L. B. Freidovich and H. K. Khalil, "Performance recovery of feedback-linearization-based designs," *IEEE Trans. Autom. Control*, vol. 53, no. 10, pp. 2324–2334, Nov. 2008.
[26] R. W. Erickson and D. Maksimovic, *Fundamentals of Power Electronics*. New York, NY, USA: Springer, 2001.
[27] S. Bacha, I. Munteanu, and A. I. Bratcu, *Power Electronic Converters Modeling and Control*, vol. 454. London, U.K.: Springer, 2014.
[28] H. K. Khalil, *Nonlinear Systems: Pearson New International Edition*, Pearson Educ. Ltd., 2013.
[29] C. Zhang, Y. Yan, C. Wen, J. Yang, and H. Yu, "A nonsmooth composite control design framework for nonlinear systems with mismatched disturbances: Algorithms and experimental tests," *IEEE Trans. Ind. Electron.*, vol. 65, no. 11, pp. 8828–8839, Nov. 2018.
[30] P. Magne, B. Nahid-Mobarakeh, and S. Pierfederici, "Dynamic consideration of DC microgrids with constant power loads and active damping system—A design method for fault-tolerant stabilizing system," *IEEE J. Emerg. Sel. Topics Power Electron.*, vol. 2, no. 3, pp. 562–570, Sep. 2014.
[31] J. Wang and D. Howe, "A power shaping stabilizing control strategy for DC power systems with constant power loads," *IEEE Trans. Power Electron.*, vol. 23, no. 6, pp. 2982–2989, Nov. 2008.

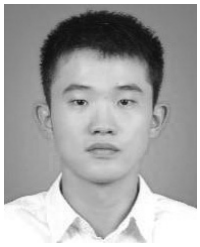

Pengfeng Lin (S'16) received the B.S. and M.S. degrees in electrical engineering from Southwest Jiaotong University, China, in 2013 and 2015, respectively. He is currently pursuing the Ph.D. degree with the Interdisciplinary Graduate School, Energy Research Institute, Nanyang Technological University, Singapore. His research interests include energy storage systems, hybrid ac/dc microgrids, and electrical power system stability analyzes.

Chuanlin Zhang (M'14) received the B.S. degree in mathematics and the Ph.D. degree from the School of Automation, Southeast University, Nanjing, China, in 2008 and 2014, respectively. He was a visiting Ph.D. student with the Department of Electrical and Computer Engineering, University of Texas at San Antonio, USA, from 2011 to 2012 and a Visiting Scholar with the Energy Research Institute, Nanyang Technological University, Singapore, from 2016 to 2017 and with Advanced Robotics Center, National University of Singapore from 2017 to 2018. Since 2014, he has been with the College of Automation Engineering, Shanghai University of Electric Power, Shanghai, where he is currently an Associate Professor.

He is the Principal Investigator of several research projects, including Leading Talent Program of Shanghai Science and Technology Commission and Chenguang Program by the Shanghai Municipal Education Commission. His research interests include nonlinear system control theory and applications for power systems. He was a recipient of the Best Poster Paper Award from the 3rd International Federation of Automatic Control International Conference on Intelligent Control and Automation Science in 2013. He serves as a Guest Editor for *Energies*.

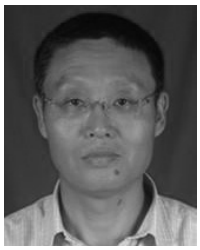

Peng Wang (M'00–SM'11–F'18) received the B.Sc. degree in electrical engineering from Xian Jiaotong University, China, in 1978, the M.Sc. degree in electrical engineering from the Taiyuan University of Technology, China, in 1987, and the M.Sc. and Ph.D. degrees in electrical engineering from the University of Saskatchewan, Canada, in 1995 and 1998, respectively. He is currently a Professor with Nanyang Technological University, Singapore.

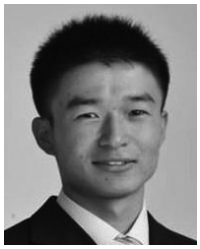

Jianfang Xiao (S'11–M'16) received the B.Sc. degree (First Class Hons.) in mechanical engineering from the School of Mechanical and Aerospace Engineering, Nanyang Techonological Univesity (NTU), in 2011 and the Ph.D. degree in electrical engineering from the School of Electrical and Electronic Engineering, NTU, in 2015, where he is currently a Research Fellow with the Energy Research Institute @ NTU.